Key Points:
- Noah-MP-PHS improves the water and carbon simulations over the default soil hydraulics schemes, especially under dry soil conditions
- Noah-MP-PHS captures different plant hydraulic behaviors between the "cavitation risk-averse" maple and the "cavitation risk-prone" oak
- Plant water storage plays a vital role in water and carbon fluxes and relieves xylem hydraulic stress during soil moisture dry-down periods

Supporting Information:
Supporting Information may be found in the online version of this article.

Correspondence to:
Z.-L. Yang and A. M. Matheny,
liang@jsg.utexas.edu;
ashley.matheny@jsg.utexas.edu

Representation of Plant Hydraulics in the Noah-MP Land Surface Model: Model Development and Multiscale Evaluation

Lingcheng Li[1], Zong-Liang Yang[1], Ashley M. Matheny[1], Hui Zheng[2], Sean C. Swenson[3], David M. Lawrence[3], Michael Barlage[4], Binyan Yan[1], Nate G. McDowell[5], and L. Ruby Leung[5]

[1]Jackson School of Geosciences, University of Texas at Austin, Austin, TX, USA, [2]Institute of Atmospheric Physics, Chinese Academy of Sciences, Beijing, China, [3]Climate and Global Dynamics Laboratory, National Center for Atmospheric Research, Boulder, CO, USA, [4]Environmental Modeling Center, NOAA/NWS/NCEP, College Park, MD, USA, [5]Atmospheric Sciences and Global Change Division, Pacific Northwest National Laboratory, Richland, WA, USA

Abstract Plants are expected to face increasing water stress under future climate change. Most land surface models, including Noah-MP, employ an idealized "big-leaf" concept to regulate water and carbon fluxes in response to soil moisture stress through empirical soil hydraulics schemes (SHSs). However, such schemes have been shown to cause significant uncertainties in carbon and water simulations. In this paper, we present a novel plant hydraulics scheme (PHS) for Noah-MP (hereafter, Noah-MP-PHS), which employs a big-tree rather than big-leaf concept, wherein the whole-plant hydraulic strategy is considered, including root-level soil water acquisition, stem-level hydraulic conductance and capacitance, and leaf-level anisohydricity and hydraulic capacitance. Evaluated against plot-level observations from a mature, mixed hardwood forest at the University of Michigan Biological Station and compared with the default Noah-MP, Noah-MP-PHS better represents plant water stress and improves water and carbon simulations, especially during periods of dry soil conditions. Noah-MP-PHS also improves the asymmetrical diel simulation of gross primary production under low soil moisture conditions. Noah-MP-PHS is able to reproduce different patterns of transpiration, stem water storage and root water uptake during a 2-week dry-down period for two species with contrasting plant hydraulic behaviors, i.e., the "cavitation risk-averse" red maple and the "cavitation risk-prone" red oak. Sensitivity experiments with plant hydraulic capacitance show that the stem water storage enables nocturnal plant water recharge, affects plant water use efficiency, and provides an important buffer to relieve xylem hydraulic stress during dry soil conditions.

Plain Language Summary Plants regulate transpiration dynamically through the stomatal aperture, which, in many cases, is governed by plant water status and hydraulic properties. Plant hydraulics describes the mechanics of water movement through plant vascular systems, which is the culmination of emergent phenotypical hydraulic functional traits at the leaf, stem, and root levels. Such physiological mechanisms are excluded in most land surface models, which typically represent plant water stress through empirical soil hydraulics schemes (SHSs) based on either soil water content or soil water potential. In this study, we present a novel plant hydraulics scheme (PHS) to represent plant water stress and the regulation of stomatal conductance for use in the Noah-MP land surface model. Our results show Noah-MP-PHS performs better in its water and carbon simulations than the default Noah-MP with traditional SHSs, especially under dry soil conditions. Noah-MP-PHS also successfully captures the different plant hydraulic behaviors between the "cavitation risk-averse" red maple and the "cavitation risk-prone" red oak. Sensitivity experiments also highlight the vital role played by plant water storage in water and carbon simulations in terms of buffering xylem hydraulic stress during soil moisture dry-down periods. The incorporation of a holistic, whole-plant hydraulic strategy, along with hydraulic trait-based vegetation representation, can serve to improve simulations of carbon and water fluxes, particularly in cases of drought and other related disturbances.

1. Introduction

Transpiration by plants is the dominant component of total terrestrial evapotranspiration (Good et al., 2015; Jasechko, 2013; Schlesinger et al., 2014). This process couples the water and carbon cycles and controls surface energy partitioning, thus playing a principal role in land surface and atmosphere/climate feedbacks (Bonan et al., 2008; Matheny et al., 2014a). A warming climate is expected to intensify the global hydrological cycle and induce more frequent and severe droughts (Dai, 2013; Li et al., 2020). Rising temperature will likewise cause an increase in atmospheric vapor pressure deficit (Grossiord et al., 2020). Plants, therefore, are expected to face more hydroclimatic stresses due to decreasing soil water supply alongside increasing atmospheric demand (Anderegg et al., 2012, 2018; McDowell et al., 2008). It is crucial to understand and simulate the dynamics of transpiration in order to better predict ecosystem-atmosphere feedbacks in water, carbon, and energy exchange (Allen et al., 2010; Bonan et al., 2008; Choat et al., 2012; Lemordant et al., 2018; Sperry et al., 2016).

As a key component of Earth system models (ESMs), land surface models (LSMs) simulate water, carbon, and energy fluxes, and are used for drought/flood prediction, weather forecasts, and climate prediction (Bonan & Doney, 2018; Yang et al., 2011). The majority of LSMs use an idealized "big-leaf" to represent all vegetation functions as a single leaf or a pair of leaves (sunlit and shaded) (Luo et al., 2018). Within the big-leaf framework, LSMs do not resolve water-state variables within plants and consequently do not have the ability to explicitly represent the plant water-stress status. Therefore, most LSMs typically parameterize the effects of soil water stress on vegetation and thus surface fluxes (i.e., water, carbon, and energy fluxes) using empirical functions based on either soil water content or soil water potential (Egea et al., 2011; Powell et al., 2013; Sitch et al., 2015; Verhoef & Egea, 2014). These traditional schemes, which we refer to as soil hydraulics schemes (SHSs), depend on soil hydraulic properties and a few plant functional related parameters (e.g., root distribution), but the role of plant traits (e.g., xylem conductivity) in controlling transpiration is largely ignored (Christoffersen et al., 2016). Many such models are satisfactory when soil moisture is adequate for transpiration, but most are unable to simulate water and carbon fluxes well under water-limited conditions (e.g., Calvet et al., 1998; Grant et al., 1999; Tuzet et al., 2003). Additionally, these LSMs fail to capture the asymmetry of daytime water and carbon fluxes under conditions of low soil moisture content, resulting in underestimation and overestimation of fluxes in the morning and afternoon, respectively (Matheny et al., 2014a; Tuzet et al., 2003). Therefore, SHS functions have been shown to contribute significant uncertainty to water and carbon simulations by LSMs (Dirmeyer et al., 2006; Kennedy et al., 2019; Niu et al., 2011; Trugman et al., 2018, 2019a).

Transpiration is regulated dynamically through the stomatal aperture, which, in many cases, is governed by water status and plant hydraulic properties (Anderegg et al., 2018; Buckley, 2005; Grant et al., 2006; Matheny et al., 2017; Skelton et al., 2015; Sperry, 2000). Water movement through plant vascular systems is regulated by the whole-plant hydraulic strategy, which is the culmination of emergent phenotypical hydraulic functional traits at the leaf, stem, and root levels (Matheny et al., 2017; McCulloh et al., 2019). At the shoot-level, plants regulate stomatal conductance during water stress across a continuum from relatively isohydric regulation in which rapid stomatal closure is associated with a smaller range of experienced leaf water potential, to relatively anisohydric regulation with higher stomatal conductance and a larger range of experienced leaf water potential. Most plants operate along a range of intermediate strategies between these two extremes (Blackman, 2018; McDowell et al., 2008; Skelton et al., 2015; Zhu et al., 2018), and relative anisohydricity can vary seasonally and interannually (Hochberg et al., 2018; Wu et al., 2020). At the stem level, plants differ in their xylem architecture, including ring-porous, diffuse-porous, and tracheid-based types (Matheny et al., 2017; Oren et al., 1999). The diversity of xylem architecture and physiology alongside numerous other vessel traits (e.g., vessel diameter, density and interconnectedness) determine xylem hydraulic functioning and its resistance to hydraulic impairment (cavitation) (Choat et al., 2012; Pockman & Sperry, 2000). The ability of a plant to store water, or its hydraulic capacitance, likewise plays a critical role in regulating the water status and tree function on time scales ranging from diel to seasonal (Matheny et al., 2015, 2016; Yan et al., 2020). Plant hydraulic regulation also arises from the properties of root systems and the rhizosphere, such as rooting depth and vertical distribution, lateral extent and competitive dynamics, fine root area, water extraction efficiency, mycorrhizal interactions, and hydraulic redistribution (Allen, 2009; Canadell et al., 1996, 2007; Reichstein et al., 2014; Wullschleger et al., 2014). The incorporation

of a holistic, whole-plant hydraulic strategy in place of the more traditional semiempirical SHS approach, along with hydraulic trait-based vegetation representation, can serve to improve simulations of carbon and water fluxes, particularly in cases of drought and other disturbances (Christoffersen et al., 2016; Kennedy et al., 2019; Mirfenderesgi, 2019).

Mechanistic modeling of plant hydraulics has advanced in recent decades and has shown clear evidence of providing a better representation of the vegetative regulation of carbon and water fluxes (Anderegg et al., 2018; Anderegg & Martin, 2020; Hunt et al., 1991; Mackay et al., 2015; McDowell et al., 2019; Mencuccini et al., 2019). There are three broad categories of plant hydraulics models, although all vary in their parameterization and implementation (see Appendix A for details). The first category of model is the pipe model (PPM), which treats the water movement within vascular conduits as laminar flow through pipes (Lehnebach et al., 2018; McCulloh et al., 2003; Shinozaki et al., 1964a, 1964b). A PPM commonly simulates water flow based on the Hagen–Poiseuille law and allometric scaling laws, and is typically applied in tree-level simulations (Mrad et al., 2018; Roderick & Berry, 2001; Savage et al., 2008). The second category is the electrical analogy model (EAM), which conceptualizes water flow through plants as being analogous to the current through an electric circuit with series of resistance and/or capacitance (Sperry et al., 1998). The third category is the porous media model (PMM), which assumes that water movement through interconnected tracheids or xylem vessels resembles porous media flow (Bohrer et al., 2005; Chuang et al., 2006). PMMs can describe in detail the spatiotemporal dynamics of a tree's hydraulic system, but at the cost of substantial computational and parametric demands. Among these three types, EAMs require relatively few parameters and have low computational demands, making them easier to apply within large-scale simulations.

Given the advancements in theory development, physics-based models, and data availability (e.g., in situ plant hydraulic traits and vegetation water status-related remote-sensing observations), mechanistic representations of plant hydraulic processes are increasingly being incorporated into LSMs to improve water and carbon simulations (Christoffersen et al., 2016; Eller et al., 2020; Hickler et al., 2006; Kennedy et al., 2019; Luo et al., 2013; Yan et al., 2020). One of the earliest examples for considering plant hydraulics in LSMs dates back to the work of Sellers et al. (1986); they employed "leaf water potential" in describing the Simple Biosphere (SiB) model, although SiB did not account for stem hydraulic capacitance. Recent examples include the Community Land Model, version 5 (CLM5; Kennedy et al., 2019) and the Joint UK Land Environment Simulator (Eller et al., 2020). However, relatively few new LSMs consider whole-plant hydraulic strategies, nor do they include explicit representation of plant hydraulic capacitance. In this paper, we present a novel EAM-type plant hydraulics scheme (PHS; Williams et al., 1996; Xu et al., 2016) for land surface modeling within the community Noah land surface model with multiparameterization options (Noah-MP) (Cai et al., 2014; Liang et al., 2019; Niu et al., 2011; Yang et al., 2011; Zheng et al., 2019, 2020). Noah-MP is a primary model employed in the NASA Land Information System (Kumar et al., 2006), the next phase North American Land Data Assimilation System (Xia et al., 2012), the Weather Research and Forecasting model (Skamarock et al., 2019), and the National Water Model (Cosgrove et al., 2016). Noah-MP is also widely used for operational weather and climate predictions (e.g., NOAA/National Centers for Environmental Prediction). This paper aims to answer the following questions:

1. Can PHS better represent plant water stress during dry soil conditions and correspondingly improve water and carbon simulations over the traditional SHSs?
2. Can PHS capture the asymmetrical diel cycles of transpiration and gross primary production under low soil moisture conditions?
3. Can PHS replicate different hydraulic behaviors between species with different hydraulic strategies (i.e., relatively isohydric vs. relatively anisohydric)?
4. Does plant hydraulic capacitance within PHS play a vital role in water and carbon simulations?

Specifically, section 2 describes the default SHSs of the host model (i.e., Noah-MP) and introduces an appropriate PHS for use in Noah-MP. Section 3 presents datasets and experimental design. Model simulation results are examined in section 4, followed by discussion and conclusions in section 5.

2. Model Description

The Noah-MP land surface model is used here as the host model. This section first describes the vital role of plant water-stress factor (β) in water and carbon simulations by regulating photosynthesis and stomatal conductance. We present three traditional soil hydraulics schemes of β parameterization in the default Noah-MP. Then, we introduce the newly developed plant hydraulics scheme for Noah-MP.

2.1. Stomatal Conductance and Plant Water-Stress Factor (β)

In Noah-MP, the Ball–Berry type stomatal conductance (g_s, μmol H_2O/m^2/s; Ball et al., 1987; Collatz et al., 1991; Niu et al., 2011; Sellers et al., 1996) is regulated through the rate of photosynthesis per unit leaf area index (LAI) (A, μmol CO_2/m^2/s)

$$g_s = m \frac{A}{c_{air} / P_{air}} \frac{e_{air}}{e_{sat}(T_v)} + g_{min},$$
(1)

where m is a plant functional type dependent parameter, c_{air} (Pa) is the CO_2 partial pressure at the leaf surface, P_{air} (Pa) is the atmospheric pressure, e_{air} (Pa) is the vapor pressure at the leaf surface and e_{sat} (Pa) is the saturation vapor pressure inside leaf at the vegetation temperature T_v, and g_{min} (μmol/m^2/s) is the minimum stomatal conductance. Photosynthesis is calculated for sunlit and shaded leaves to give the sunlit and shaded leaf stomatal conductance, respectively.

A plant water-stress factor (β) is then applied to affect the photosynthesis via the maximum carboxylation (V_{cmax}, μmol CO_2/m^2/s):

$$V_{cmax} = \beta V_{cmax,ww},$$
(2)

$$V_{cmax,ww} = V_{cmax,25} f(N) f(T_v) \alpha_{vmax}^{\frac{T_v - 25}{10}},$$
(3)

where $V_{cmax,ww}$ is the maximum carboxylation when vegetation is under well-watered conditions, α_{vmax} is the temperature sensitive parameter, $f(T_v)$ is a function that mimics thermal breakdown of metabolic processes (Collatz et al., 1991), and $f(N)$ is a foliage nitrogen factor, which is equal to 1 in this version of Noah-MP, assuming the foliage nitrogen is saturated. The nitrogen dynamics is considered in the Noah-MP-CN version of the model [for details, refer to Cai et al. (2016) and Liang et al. (2020)].

The plant water-stress factor plays a crucial role in regulating photosynthesis and stomatal conductance in the model, and therefore affects the water and carbon simulations. In the default Noah-MP, there are three β schemes, which are all empirical functions based on either soil moisture or soil water potential (i.e., SHS; see section 2.2). The newly developed plant hydraulics scheme (i.e., PHS; see section 2.3) based on plant hydraulics theory uses leaf water potential to formulate β with higher fidelity.

2.2. Traditional SHSs in Noah-MP

Transpiration (TR) is supported by whole-plant water extraction, which is partitioned into the root water uptake (Q_i) from the ith root-zone soil layer,

$$Q_i = \frac{r_i \cdot w_i}{\beta} \cdot \text{TR},$$
(4)

where β is calculated as the root ratio (r_i) weighted average of the soil layer wetness factor (w_i) among N_r soil layers:

$$\beta = \sum_{i=1}^{N_r} r_i \, w_i,$$
(5)

Three default SHSs have different parameterizations for w_i ($0 \leq w_i \leq 1$):

(1) The Noah-type SHS (Chen & Dudhia, 2011) is represented as a function using soil moisture ($\theta_{\text{liq},i}$),

$$w_i = \frac{\theta_{\text{liq},i} - \theta_{\text{wilt}}}{\theta_{\text{ref}} - \theta_{\text{wilt}}}, \tag{6}$$

where θ_{wilt} and θ_{ref} (m^3/m^3) are soil moisture at the wilting point and a reference soil moisture at field capacity, respectively.

(2) The CLM-type SHS (Oleson et al., 2004; Yang & Dickinson, 1996) depends on a function using soil matric potential,

$$w_i = \frac{\psi_{\text{wilt}} - \psi_i}{\psi_{\text{wilt}} - \psi_{\text{sat}}}, \tag{7}$$

where $\psi_i = \psi_{\text{sat}} \cdot \left(\frac{\theta_{\text{liq},i}}{\theta_{\text{sat}}}\right)^{-b}$ is the matric potential of the soil layer i, ψ_{sat} is the saturated matric potential, ψ_{wilt} is the soil matric potential reaching the wilting point, and b is an empirical factor related to soil texture.

(3) The SSiB-type SHS (Xue et al., 1991) is also based on soil matric potential:

$$w_i = 1 - e^{-c_2 \ln\left(\psi_{\text{wilt}}/\psi_i\right)}, \tag{8}$$

where c_2 is a slope factor ranging from 4.36 for crops to 6.37 for broadleaf shrubs.

2.3. Plant Hydraulics Scheme for Noah-MP

As summarized in the section 1 and Appendix A, there are three commonly used models for plant hydraulics processes. Among them, resistance-capacitance models (RCMs) require relatively fewer parameters and demand relatively less computational time. Therefore, RCMs are highly suitable for use within LSMs or ESMs on a large spatial scale.

In this study, we present a novel RCM-type PHS for use in Noah-MP based primarily on the works of Xu et al. (2016) and Williams et al. (1996). This PHS considers plant water storage in the stem and leaves. Biomass hydraulic capacitance regulates water economy and tree function on time scales ranging from diel to seasonal (Yan et al., 2020), by maintaining daily transpiration, buffering drought impacts on xylem embolism and consequent hydraulic failure, and supporting leaf growth in the dry season for seasonally deciduous trees (Goldstein et al., 1998; Huang et al., 2017; Meinzer, 2003).

The governing equations of the PHS are primarily based on the conservation of mass and Darcy's law, describing the relationships between plant water potential and plant water storage, plant water potential and hydraulic conductance, leaf water potential, and plant water-stress dynamics. Details are provided in the sections 2.3.1, 2.3.2, 2.3.3, 2.3.4.

2.3.1. Water Flux from Soil to Root

Water flux (Q_i, mm/s) from soil to root within each soil layer i of the root zone is driven by the water potential gradient between root water potential and soil matric potential ($\Psi_{\text{soil},i}$, mm). For simplicity, the roots and stem are directly linked as one component at the base of the stem (Figure 1b). Root water potential within each soil layer drives the stem water potential (Ψ_{stem}, mm) at the ground surface. Soil-to-root water flux in the ith layer is calculated following Darcy's law:

$$Q_i = k_{\text{soil-root},i} \times \left(\Psi_{\text{soil},i} - \Psi_{\text{stem}} - \Psi_{s,i}\right), \tag{9}$$
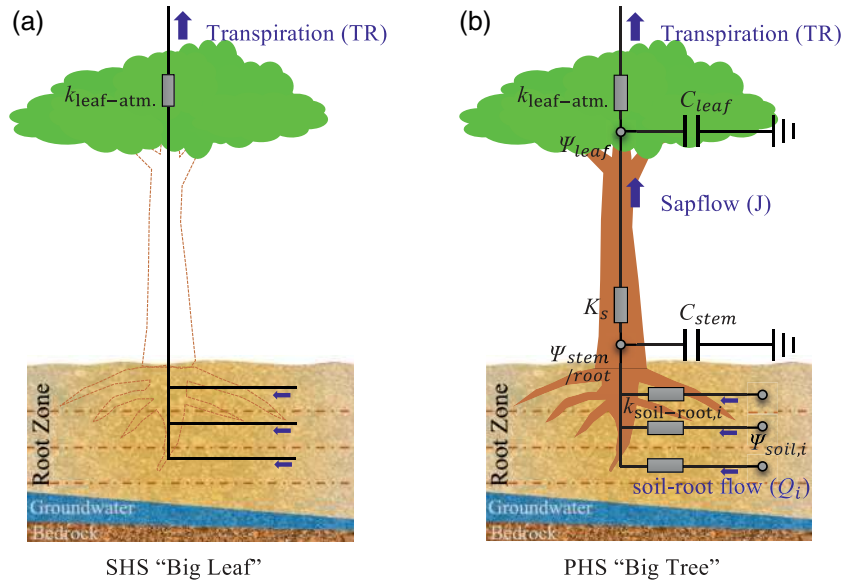
Figure 1. (a) Schematic representation of the traditional soil hydraulics scheme (SHS "big leaf"). Such models assume leaves can directly access soil water from the root zone, distributing transpiration based on the wetness factor [equations (6)–(8)] at each root-zone layer. (b) Schematic representation of the plant hydraulics scheme (PHS "big tree"), with physical representation of roots, stem, and leaf, separately. $k_{\text{leaf}-\text{atm.}}$ denotes the conductance from leaf to canopy air, consisting of leaf boundary conductance and stomatal conductance.

$$Q = \sum_{i=1}^{N_r} Q_i, \tag{10}$$

where Q is the total water flux calculated as the sum of water flux at each layer Q_i (mm/s); and $\Psi_{s,i}$ (mm) represents the specific gravitational water potential drop from soil layer i to the base of the stem, and equals the depth from the center of the soil layer i to the ground ($h_{s,i}$, mm).

$k_{\text{soil-root},i}$ (s^{-1}) is the hydraulic conductance from soil to root at layer i and is calculated following Katul et al. (2003):

$$k_{\text{soil-root},i} = K_{\text{soil,sat}} \times \left(\frac{\theta_{\text{liq},i}}{\theta_{\text{sat}}} \right)^{2b+3} \times \frac{\sqrt{\text{RAI}_i}}{\pi \times d_i}, \tag{11}$$

where $K_{\text{soil,sat}}$ is the hydraulic conductance at satuation, $\theta_{\text{liq},i}$ represents the volumetric soil moisture in the ith layer, θ_{sat} is the volumetric soil moisture at saturation, and d_i is the depth of the ith soil layer.

Soil water potential $\Psi_{\text{soil},i}$ (mm) is calculated based on Clapp and Hornberger (1978):

$$\Psi_{\text{soil},i} = \Psi_{\text{soil},sat} \times \left(\frac{\theta_{\text{liq},i}}{\theta_{\text{sat}}} \right)^{-b}, \tag{12}$$

where b is an empirical factor determined by soil texture.

The root area index RAI$_i$ in soil layer i is based on the root fraction r_i multiplied by the total root area (RAI) (Kennedy et al., 2019), which is the sum of the stem area index (SAI) and LAI, multiplied by the root-to-shoot ratio ($f_{\text{root-shoot}}$):

$$\text{RAI}_i = f_{\text{root-shoot}} \cdot \left(\text{LAI} + \text{SAI} \right) \cdot r_i \tag{13}$$

In this paper, hydraulic redistribution is prevented by setting Q_i as 0 if the soil water potential in the ith layer is lower than the root water potential (it can be turn on when needed).

2.3.2. Water Flux from Stem to Leaf

Sap flux from the base of the stem to the leaf J (mm/s) is computed based on Darcy's law and is dependent on the xylem hydraulic conductivity K_s (mm/s), sapwood-area index S_{sap} (sapwood area per ground area, m^2/m^2), and plant canopy height h_c (mm):

$$J = \frac{K_s \times S_{sap} \times \left(\Psi_{stem} - \Psi_{leaf} - \Psi_c \right)}{a_1 \cdot h_c},$$ (14)

where Ψ_{leaf} (mm) is the leaf water potential, Ψ_c (mm) represents the specific gravitational water potential drop from the ground to the canopy (i.e., h_c), $a_1 \cdot h_c$ represents the length of the water flow route, and a_1 is an empirical parameter;

$$K_s = K_{s,sat} \times \left[1 + \left(\frac{\Psi_{stem}}{P_{50}} \right)^{a_2} \right]^{-1},$$ (15)

where $K_{s,sat}$ (mm/s) denotes the saturated xylem hydraulic conductivity, P_{50} is the stem water potential at 50% loss of conductivity, and a_2 is an empirical parameter.

2.3.3. Update of Water Potentials

Based on water balance, changes in the leaf and stem water storages lead to changes in the leaf and stem water potentials,

$$\frac{d\Psi_{stem}}{dt} = \frac{Q - J}{C_{stem} \times V_{sap}},$$ (16)

$$\frac{d\Psi_{leaf}}{dt} = \frac{J - TR}{C_{leaf} \times LAI},$$ (17)

where dt (s) is the calculation time step; C_{leaf} (mm/mm) and C_{stem} (m^{-1}) are the leaf and stem water capacitances, respectively; and LAI (m^2/m^2) and V_{sap} (m^3/m^2) are the leaf area index and sapwood volume index, respectively.

2.3.4. Calculation of Plant Water Stress

Leaf water potential is used to formulate the plant water stress (β) with higher fidelity (Xu et al., 2016):

$$\beta = \left[1 + \left(\frac{\psi_{leaf}}{TLP} \right)^{a_3} \right]^{-1},$$ (18)

where TLP (mm) is the turgor loss point, i.e., Ψ_{leaf} when the photosynthetic capacity rate halves, and a_3 is an empirical parameter.

These PHS parameters are summarized in Table 1.

3. Methods

3.1. Data

Model evaluation was conducted based on observations from the University of Michigan Biological Station (UMBS) located in Northern Lower Michigan, USA. The annual average precipitation of this site is 805 mm, and its annual mean temperature is near 6.8°C (Matheny et al., 2014b). The soil texture at

Table 1
Parameters Added in the Plant Hydraulics Scheme

Parameter	Description	Units
TLP	Turgor loss point, corresponding leaf water potential when photosynthetic capacity rate halves	mm
C_{leaf}	Leaf water capacitance	mm/mm
$K_{s,sat}$	Sapwood-area-specific saturated xylem hydraulic conductivity	mm/s
P_{50}	Stem water potential at 50% loss of conductivity	mm
C_{stem}	Stem water capacitance	m^{-1}
S_{sap}	Specific sapwood area index	m^2/m^2
V_{sap}	Specific sapwood volume index	m^3/m^2
h_c	Canopy height	mm
a_1	Empirical parameter controlling length of water flow route	Dimensionless
a_2	Empirical parameter controlling xylem hydraulic conductance	Dimensionless
a_3	Empirical parameter controlling plant water stress	Dimensionless
$f_{root-shoot}$	Fine root area to shoot area (i.e., leaf area + stem area) ratio	m^2/m^2

UMBS is dominated by extremely well-drained spodosols and contains 92% sand, 7% silt, and 1% clay (He et al., 2013). Mean canopy height is approximately 29 m. Fluxes, meteorological forcing, and tree-level and plot-level biological data are available from the AmeriFlux database (site-ID: US-UMB). Observations used in this study include soil moisture (m^3/m^3; at the depths of 5, 15, 30, 60, 100, 200, and 300 cm), gross primary production (μmol $CO_2/m^2/s$), and sap flux. Matheny et al. (2014b) scaled measured values of tree-level sap flux to the equivalent plot-level sap flux with good agreement (see details in Matheny et al., 2014b). Here, we use the upscaled sap flux as a proxy of transpiration to compare with the model simulations. It should be noted that, commonly, there is a time lag between sap flux and transpiration, typically on the order of 30–90 min. We adjusted the sap flux time series to match its peak with the peak of the net radiation based on half-hourly data for each day. Considering GPP and transpiration generally cooccur (for C_3 plants) over the daytime, we calculated the correlation coefficients (CCs) between the GPP and original/adjusted sap flux. The CC increases from 0.78 to 0.85 after adjustment, indicating that the adjustment approach should be reasonable, albeit with some limitation.

Tree-level measurements were also used to evaluate our tree-level simulations. Matheny et al. (2016) found that during an interstorm dry period [day of year (DOY) 211–224 in 2014], red maple (*Acer rubrum*) sap flux and stem water storage were strongly reduced, while red oak (*Quercus rubra*) water fluxes were only slightly affected. The diverging hydraulic strategies (Matheny et al., 2016) between red oak (deep roots, large xylem vessels, anisohydric) and red maple (shallow roots, small xylem vessels, isohydric) provide an ideal experiment to test our newly developed PHS. Leaf water potential was measured in canopy-top leaves exposed to full sun of mature red oak and red maple trees using a pressure chamber (Model 600 PMS Instrument Co., Corvallis, OR, USA; see details in Matheny et al., 2016). Leaf water potential measurements were made at roughly 06:00 (dawn), 13:30 (noon), and 16:00 (afternoon) from June 23 to July 12, 2014 (DOY 174–193). Stem water storage and sap flux were continuously monitored in one mature, canopy-dominant individual of each species (i.e., one red oak and one red maple) in 2014 (Matheny et al., 2016). Sap flux was also adjusted to match the peak of net radiation. The canopy height, crown area, and sapwood area for the red maple (oak) tree are 27.4 (31.3) m, 40.1 (50.1) m^2, and 252.3 (342.3) cm^2, respectively.

The model soil hydraulic properties and root vertical distribution were set based on site observations. Soil hydraulic parameters were derived from pedotransfer functions (Saxton et al., 1986) using the percentages of sand, silt, and clay (92%, 7%, and 1%) for our plots (He et al., 2013). Specifically, we set the soil moisture at the wilting point as 0.033 m^3/m^3, the reference soil moisture at field capacity as 0.099 m^3/m^3, and the soil porosity as 0.265 m^3/m^3.

By default, the fine root ratio at each layer is proportional to the soil layer thickness (i.e., 10, 30, 60, and 100 cm for the first to fourth soil layer), i.e., evenly distributed fine root density at each layer (i.e., 0.05, 0.15,

Table 2
Model Setup for Plot-Level and Tree-Level Simulations

	Plot-level	Red maple	Red oak
Period	Growing season in 2013 and 2014	Growing season in 2014	Growing season in 2014
Forcing	Flux tower	Flux tower	Flux tower
Soil moisture	Model simulation	First to fourth layer soil moisture observation	First to third layer soil moisture observation, constant fourth layer soil water to mimic groundwater usage
Soil layer thickness	0.1, 0.3, 0.6, 1.0 m	0.1, 0.3, 0.6, 1.0 m	0.1, 0.3, 0.6, 9.0 m
(First to fourth layer)	(total: 2 m)	(total: 2 m)	(total: 10 m)
Fine root ratio	0.33, 0.47, 0.18, 0.02	0.33, 0.47, 0.18, 0.02	0.22, 0.41, 0.28, 0.09
(First to fourth layer)	He et al. (2013)	He et al. (2013)	Bréda et al. (1995)

0.3, 0.5 for the first to fourth layer). Instead, we updated the fine root ratio based on the fine root biomass measurements at UMBS (He et al., 2013). The updated root ratios are 0.316, 0.465, 0.196, and 0.023 for the first to fourth layer, respectively (the oak simulation used a different set of root ratios; see details below).

3.2. Plot-Level and Tree-Level Experiments

We conducted plot-level simulations of about 180 ha in area and comprising 99% of the flux footprint of the US-UMB flux tower, to evaluate the newly developed PHS (Table 2). The upscaled sap flux (i.e., transpiration; see section 2.2 for details) and flux tower GPP were used to evaluate model performance and explore whether PHS could improve water and carbon simulations. We focus on the growing season of 2013–2014 (DOY 153–262 in 2013 and 191–257 in 2014).

Red maple and red oak are two codominant midsuccessional tree species at UMBS. Red maple favors a "cavitation risk-averse" hydraulic strategy, while red oak employs a "cavitation risk-prone" hydraulic strategy. These two species have different hydraulic traits within the roots, xylem, and leaves (Matheny et al., 2014b; Thomsen et al., 2013). Therefore, we have an ideal testbed to evaluate the capabilities of PHS for species with divergent hydraulic strategies. We conducted tree-level simulations for a red oak tree and a red maple tree based on tree-level measurements of transpiration and stem water storage. We focused only on the plant hydraulics process and constrained the simulations using observed soil moisture. Matheny et al. (2016) suggested that red maple predominantly uses shallow water sources, while red oak can use a deeper and less variable water source. Fan et al. (2017) summarized that the measured average rooting depth for maple and oak is 1.75 m and 5.23 m, respectively. Therefore, for the red maple simulation, we kept the same rooting depth (i.e., 2 m) and root ratios as the plot-level simulation. But for the oak simulation, we set a deeper rooting depth (i.e., 10 m), and the root ratios were based on the vertical fine root measurements of mixed pedunculate oak and sessile oak from Bréda et al. (1995). Compared with the root ratio of red maple, red oak has a larger root ratio in the third and fourth soil layer. To mimic the oak using deeper water sources, we calibrated a constant value of soil moisture for the fourth soil layer, considering there was no substantial drought affecting the groundwater during our modeling period.

3.3. Sensitivity Experiments of Plant Capacitance

As described in Appendix, there are two types of EAM, i.e., RM (resistor model. e.g., implemented in CLM5) and RCM (implemented here), frequently employed for large-scale plant hydraulics modeling. The difference between them is whether they consider plant hydraulic capacitance. To understand the role of plant water storage on the hydraulic process, we further conducted a series of tree-level sensitivity experiments during the 2014 dry-down period. These experiments applied the same experiment settings as the red maple simulation (see section 3.3), i.e., the same calibrated parameters and boundary conditions (soil moisture and forcing), but by using a series of stem hydraulic capacitance.
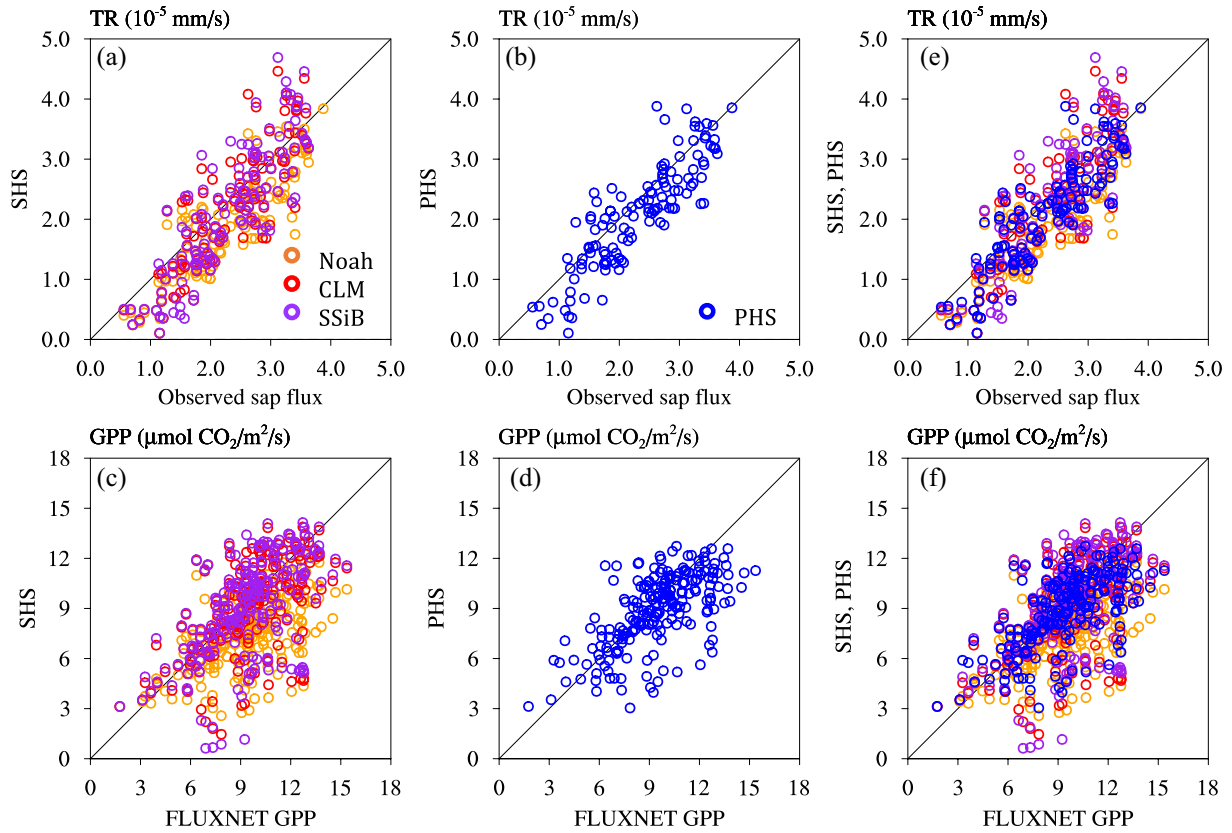
Figure 2. Comparison of daily transpiration (TR) (a, b) and GPP (c, d) simulations between SHSs and PHS. Panels (e) and (f) are the combination of panels (a) and (b) and (c) and (d), respectively. SHSs, soil hydraulics schemes; PHS, plant hydraulics scheme.

3.4. Model Calibration

We use the root-mean-square error (RMSE) and the modified Kling-Gupta Efficiency (KGE; Kling et al., 2012) to evaluate model performance. KEG computes the Euclidian distance between the ideal point and three components, including the CC, bias ratio (BR), and variability ratio (VR) [see details in Gupta et al. (2009) and Kling et al. (2012)].

Five key PHS parameters (Table 1), including TLP, $K_{s,sat}$, P_{50}, C_{stem}, and a_1, are calibrated for each of the above three experiments, i.e., one plot-level experiment, the red maple and red oak tree-level experiments. For each experiment calibration, we set ensemble runs with combinations of parameter values, and optimize the model outputs to match the observations, i.e., plot-level sap flux and GPP for the plot-level simulation, and sap flux and stem water storage of one red maple and one red oak for the tree-level simulation. Other PHS parameters are based either on measurements or the default values from Xu et al. (2016). PHS parameters are shown in Table S1.

Table 3
Statistics of Model Performance at the Daily Time Scale (Best Values are Written in Bold Type)

Scheme	Transpiration		GPP	
	RMSE	KGE	RMSE	KGE
Noah	0.60	0.62	2.96	0.49
CLM	0.57	0.54	2.44	0.54
SSiB	0.61	0.48	2.59	0.48
PHS	**0.48**	**0.72**	**2.10**	**0.62**

4. Results

4.1. Plot-Level Evaluation

4.1.1. Overall Model Performance

We evaluated four Noah-MP configurations with different water-stress schemes, i.e., the new PHS, and the three default Noah, CLM and SSiB SHSs. PHS generally shows better performance for transpiration and GPP simulations than the simulations by default SHSs. Figure 2 compares the model simulations and observations at the daily time scale, and corresponding statistics are shown in Table 3. For the daily transpiration
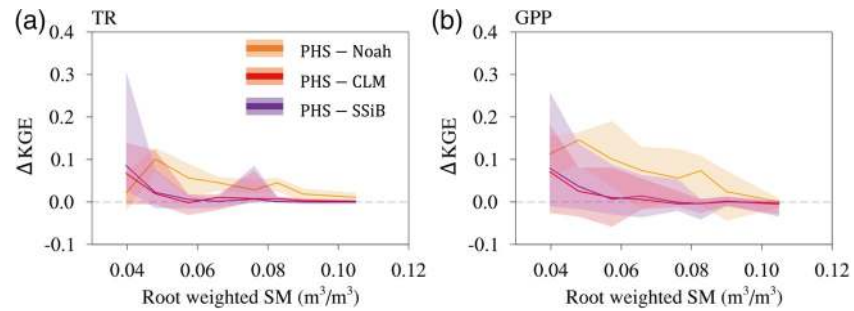
Figure 3. ΔKGE between PHS and SHSs for (a) transpiration (TR) and (b) GPP under different soil moisture (SM). The solid lines are the median of the ΔKGE in each SM interval, with the 25th and 75th percentiles shaded. Along the *x* axis are eight SM observation bins. Root-weighted SM (i.e., $\sum_1^4 \theta_{\text{liq},i} \cdot r_i$) is the sum of root fraction-weighted soil moisture at each layer. SHSs, soil hydraulics schemes; PHS, plant hydraulics scheme.

simulation, PHS shows the best performance compared with the three default SHSs, with the lowest RMSE (0.48 versus 0.60, 0.57 and 0.60×10^{-5} mm/s) and the highest KGE (0.72 versus 0.62, 0.54, and 0.48), and with particularly strong performance in terms of the CC and VR (see Table S2). For the daily GPP simulation, PHS performs better than the default SHSs, with a lower RMSE (2.10 versus 2.96, 2.44, and 2.59 μmol CO_2 /m^2/s) and a higher KGE (0.62 versus 0.49, 0.54, and 0.48), and again with particularly strong performance in terms of the CC and VR (see Table S2). Similarly, PHS also has the best performance for transpiration and GPP at the hourly time scale (Table S2 and Figure S1). Besides the transpiration and GPP, the PHS-modeled daily soil moisture is better than that simulated by the SHSs, with lower RMSE at the first, third, and fourth layer (Figure S2 and Table S2).

4.1.2. Model Performance Under Different Soil Moisture

We further analyzed the models' performances under different soil moisture conditions (Figure 3). PHS overall outperforms the SHSs as the soil becomes drier. For each day, we calculated the KGE of different schemes using the hourly data, and then computed the difference of KGE (ΔKGE) between the PHS and each default SHS (i.e., Noah, CLM, SSiB). Finally, we binned the ΔKGE using daily soil moisture observation into eight intervals (i.e., approximately 26 values of ΔKGE in each interval for each comparison between PHS and the default SHSs). Figure 3 shows the ΔKGE under different soil moisture conditions. Positive values indicate that PHS performs better (i.e., higher KGE) than the corresponding SHS. Compared with the Noah scheme, PHS shows better performance under different soil moisture for both transpiration and GPP simulations, and the drier the soil, the larger the improvement (except the driest condition for transpiration simulation). Compared with the CLM and SSiB schemes, PHS shows comparable performance for transpiration and GPP simulations under non-limiting conditions (i.e., soil moisture >0.06 m^3/m^3), but outperforms the other schemes as soil moisture becomes drier.

4.1.3. Plant Water-Stress Dynamics

Figure 4 compares the daily averaged β values between PHS and the SHSs under different soil moisture conditions. PHS simulates a larger β under dry soil conditions and hence improves model performance over three SHSs. Compared with the CLM and SSiB schemes, PHS has similar β values when soil moisture is greater than 0.06 m^3/m^3, but larger values when the soil becomes dry. When PHS is compared with the Noah scheme, the relative difference in β becomes larger with soil moisture dry-down. These β dynamics under different soil moisture conditions show similar patterns of model performance when comparing PHS with SHSs (Figure 3).

4.1.4. Diel Simulations Demo Under Dry and Wet Soil Moisture

We analyzed the diel cycles of transpiration, GPP and β on a typical wet day (DOY 227) and a dry day (DOY 235) over a dry-down period in 2013. During the wet day, PHS and the three SHSs show similar performances with similar KGE for both transpiration and GPP simulations (Figures 5a, 5c and Table S3). While under the limited water conditions, PHS shows better performance than the three SHSs with larger KGE and smaller RMSE, especially for the GPP simulation (Figures 5b, 5d and Table S3).
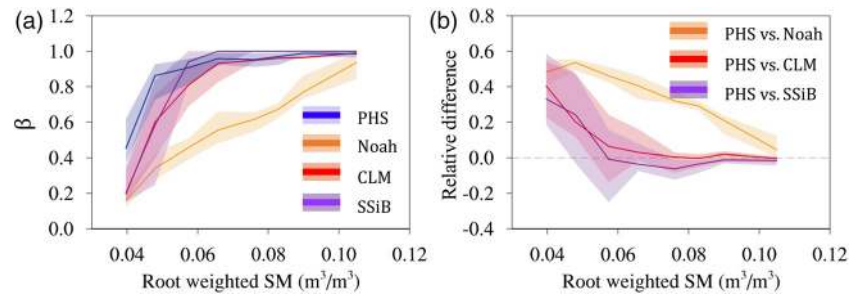
Figure 4. (a) β dynamics for four schemes and (b) the relative difference between PHS and three SHSs under different soil moisture (SM) conditions. Relative difference in (b) is computed as $\left(\beta_{PHS} - \beta_{SHS} \right) / \beta_{PHS}$. SHSs, soil hydraulics schemes; PHS, plant hydraulics scheme.

Notably, PHS also captures the asymmetrical daytime fluxes of GPP, i.e., higher fluxes in the morning than the afternoon, especially under conditions of low soil moisture content (Figures 5c and 5d). These patterns are consistent with the dynamics of PHS′ β, which shows diel and asymmetrical daytime variation (Figures 5e and 5f). However, there are no asymmetrical patterns for the SHSs′ simulations of GPP. The β values of the three SHSs show negligible variations (Figure 5e). These β values are based on the root-zone soil moisture or soil matric potential that varies slowly (on the order of days and weeks).
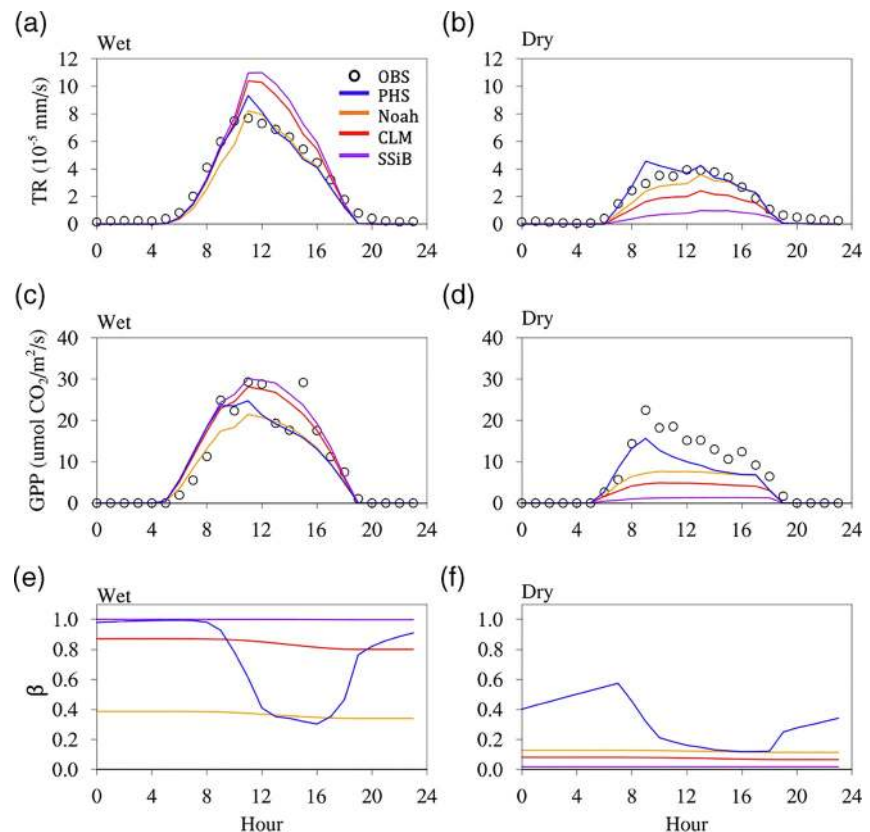

Figure 5. Diel cycles for (a, b) transpiration (TR), (c, d) GPP, and (e, f) β root water uptake on a typical (a, c, e) wet day (DOY 227 in 2013) and (b, d, f) dry day (DOY 235 in 2013).
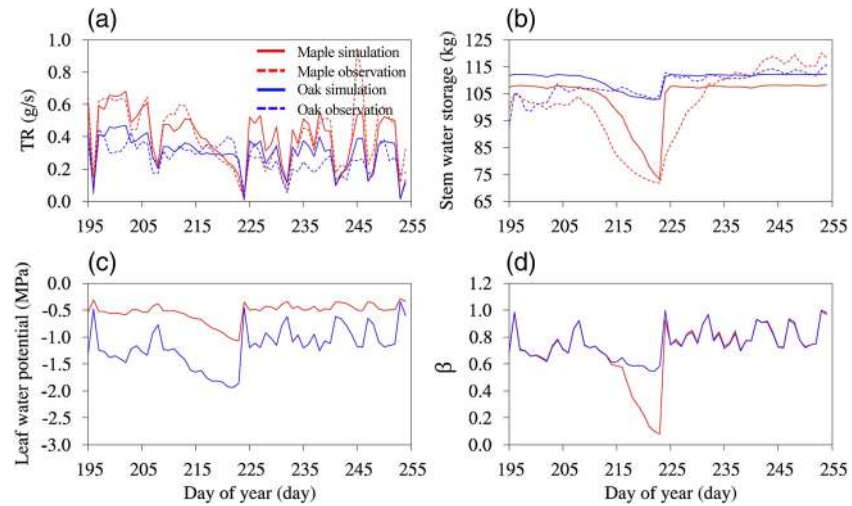
Figure 6. Daily simulations for red maple and red oak. TR is the daily transpiration. Red (blue) solid and dash curves denote maple's and oak's simulation and observation, respectively. TR, transpiration.

4.2. Tree-Level Simulations

4.2.1. Overall PHS Performance

We further applied Noah-MP-PHS in tree-level simulations and found that it successfully captures the transpiration and stem water storage for the two tree species with different hydraulic behaviors. The calibrated parameters for the red maple and red oak simulations are listed in Table S1 using observations of transpiration and stem water storage. Figure 6 shows their simulations at the daily time scale (DOY 195–254). It should be noted that PHS only simulates the variation of plant water storage, instead of the absolute value of storage. Therefore, we adjusted the simulated stem water storage to match its average with the average of observed stem storage. During the soil moisture dry-down period (i.e., DOY 209–222; Figures S3 and S4), red maple's transpiration and stem water storage were strongly affected by this decrease in soil water content, but this was not so for red oak. Based on the observations, under the limited soil moisture, transpiration for red maple gradually declined from a maximum of 0.60 g/s at DOY 2012 to 0.20 g/s at DOY 222, while oak maintained a relatively stable transpiration, with an average of around 0.33 g/s (Figure 6a). Concurrently, stem water storage in red maple fell by 29% from 101.3 to 72.2 kg, but there was less of a change in stem water storage (between 107.4 and 103.1 kg) in red oak (Figure 6b).

These divergent behaviors between red oak and red maple were well captured by the PHS simulations, with overall high KGE and low RMSE values (Table 4) for both transpiration and stem water storage simulations (Figures 6a and 6b). It is important to note that our calibrated key parameters of $K_{s,sat}$ and P_{50} are comparable with the in situ measurements. The calibrated $K_{s,sat}$ (P_{50}) is 1.00×10^{-2} mm/s and 1.50×10^{-2} mm/s (-2.00×10^5 and -1.50×10^5 mm) for red maple and red oak, respectively, which are roughly consistent with the values of 0.55×10^{-2} and 1.33×10^{-2} mm/s (-1.97×10^5 and -1.61×10^5 mm) based on field measurements for the same species (Maherali et al., 2006). Red maple's lower values of $K_{s,sat}$ and P_{50} than those of red oak are consistent with their different xylem architecture, i.e., diffuse-porous (red maple) and ring-porous (red oak). Oak's stem water storage simulation has a low KGE value of 0.27 over the whole period from DOY 195 to 254. However, the KGE increases to 0.77 without considering the period of DOY 195–205. This is because PHS failed to capture the increasing stem water storage in this period. Red maple's stem water storage observations show gradual recharge after a rain event at DOY 224, while the model shows immediate full recharge after soil moisture enhances. This discrepancy could be because the model has no mechanism to reproduce the time lag associated with vessels refilling after drought.

Table 4
Statistics of Model Performance at the Daily Time Scale over DOY 195–254.

Species	Transpiration		Stem water storage	
	RMSE	KGE	RMSE	KGE
Maple	0.10	0.82	9.38	0.54
Oak	0.08	0.70	4.89	0.27 (0.77[*])

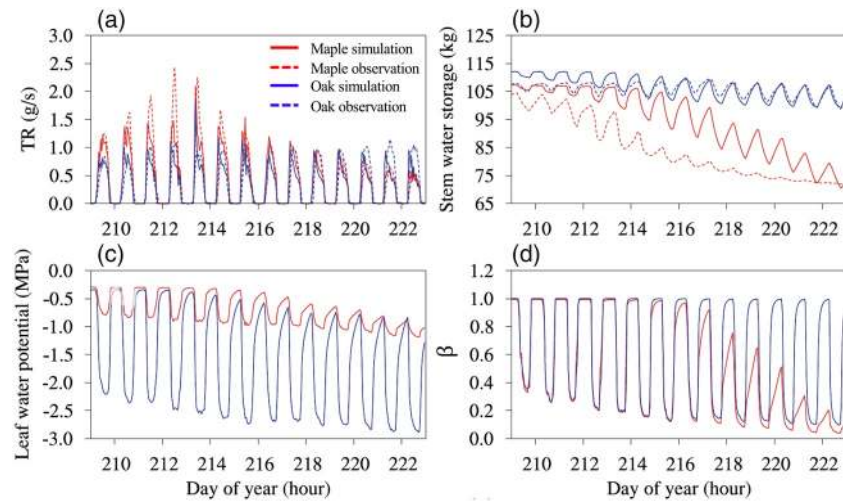[*]KGE is calculated over DOY 205–254.

Figure 7. Hourly simulations for red oak and red maple during the dry-down period. Panels (a) and (b) show comparisons between model output (solid lines) and observations (dotted lines). Observations were not available for leaf water potential or β and are therefore omitted from panels (c) and (d).

Compared with the leaf water potential of red oak, red maple's is more stable and less negative (Figure 6c), as is characteristic of its relatively isohydric strategy. The averages of leaf water potential measurements at noon for red maple and red oak are -0.51 and -1.3 MPa, respectively, over DOY 174–193. PHS simulates a comparable leaf water potential of -0.74 MPa for red maple and -2.1 MPa for red oak. The β dynamics also show a notable difference between red maple and red oak during the dry-down period. Red oak maintains a relatively larger β, keeps stomatal openness, and supports stable transpiration. However, red maple's β gradually declines, as the stomata close and transpiration is reduced.

4.2.2. Dynamics During the Dry-Down Period

Figure 7 shows the hourly time series over the dry-down period (DOY 209–222). Noah-MP-PHS reasonably simulates different hydraulic behaviors at the leaf and stem levels for these two species (see statistics at Table S4). The diel withdrawal from stem storage of red maple fell from 13.2 kg on DOY 209 to 0.73 kg on DOY 222, while red oak shows opposite patterns, with storage withdrawal rising from around 4.9 to 8.3 kg over the same period (Figure 7b). The stem water storage simulations capture their contrasting patterns. Simulated storage withdrawal of red maple dropped from 15.1 kg on DOY 217 to 8.9 kg on DOY 222, and red oak's storage withdrawal increased slightly from 6.9 kg on DOY 213 to 8.1 kg on DOY 222.

For the simulation of leaf water potential, red maple has small diel amplitudes (around 0.5 MPa)—the difference between daily maximum and minimum—and slightly dropped its daily maximum and minimum leaf water potential over the dry-down period (Figure 7c). On the other hand, the leaf water potential of red oak has larger diel amplitudes as its relatively anisohydric strategy allows for strongly negative daily minimum leaf water potential. Similar patterns of stem water potential were simulated for these two trees (Figure S5). The water-stress β, as a function of leaf water potential, shows similar patterns for these two species. Red maple gradually decreased its daily maximum β in response to the dry-down period. Red oak, which uses deeper water sources, shows few changes in β dynamics. These behaviors are consistent with their different hydraulic strategies. Red maple is more isohydric, and it uses tighter stomatal regulation, maintaining a relatively stable and high leaf water potential. Red oak is relatively more anisohydric, and regularly tolerates highly negative leaf water potential.

4.2.3. Root Water Uptake

Figure 8 shows the root water uptake (Q) of red oak and red maple during the dry-down period (DOY 209–222). Noah-MP-PHS simulates different root-level hydraulic behaviors for these two species. With limited water in the top 2 m of soil, red maple significantly reduced its Q from 0.45 g/s on DOY 209 to 0.17 g/s on DOY 222 (decrease of 62%). Concurrently, red oak reduced its Q from 0.32 to 0.25 g/s (reduction of 22%).
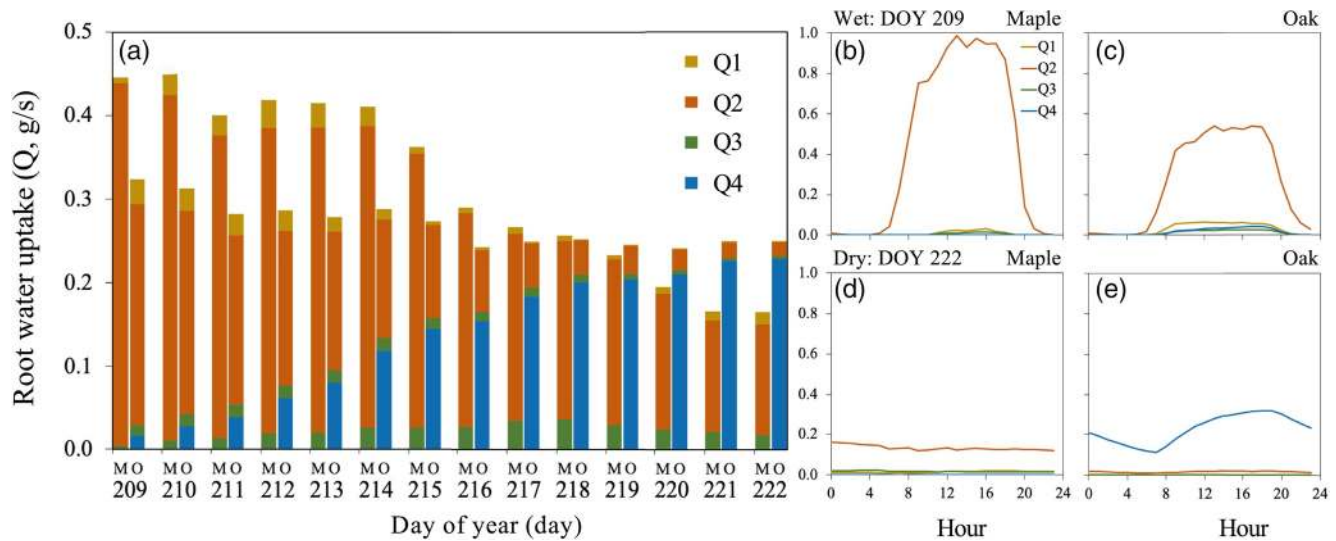
Figure 8. Root water uptake (Q) for red maple (M, left bars) and red oak (O, right bars) during the dry-down period: (a) daily Q from the first to fourth soil layer (i.e., Q1–Q4); (b–e) diel variation of Q under wet and dry conditions for these two trees.

Red maple obtained most of its water from the second soil layer, accounting for 95% of the total Q on DOY 209 and 81% on DOY 222 (Figures 8a and S6), because about half (47%) of maple's fine roots reside in this layer. For red oak, during nonwater-limited conditions, most water also came from the second soil layer, accounting for 82% on DOY 209. As the upper three soil layers dried, red oak started using more water from the wet fourth layer, increasing from only 1% on DOY 209 to 91% on DOY 222 (Figures 8a and S6).

Additionally, under the relatively wet soil conditions, red maple and red oak both absorbed the majority of their water during the daytime (i.e., 06:00–18:00; Figures 8b and 8c), which accounts for 92% and 86% of the daily total Q on DOY 209 for red maple and red oak, respectively. As the soil dried, these two began taking up more water during the nighttime (i.e., 00:00–05:00 and 19:00–23:00; Figures 8d and 8e), which accounts for 48% and 43% of the daily total Q on DOY 222 for red maple and red oak, respectively.

4.3. Sensitivity Simulations with Different Plant Capacitance

Figure 9 shows the tree-level simulations of a series of sensitivity experiments with different stem hydraulic capacitance during the dry-down period (DOY 209–222). Overall, different hydraulic capacitance induced noticeable differences in simulations of water and carbon variables, and their differences become larger as the soil dried. Specifically, larger hydraulic capacitance can buffer short-term variation in hydraulic demand and subsequently transpiration (i.e., leaves) (Figure 9a), which enables greater stomatal conductance (daytime β in Figure 9b). Therefore, larger hydraulic capacitance can supply more transpiration (Figure 9c) and promote increased carbon gain (Figure 9d). However, smaller hydraulic capacitance appears to promote higher water use efficiency (WUE, g C/kg H_2O; Figure 9e)—the ratio between GPP and transpiration.

Larger hydraulic capacitance also supports less-negative daily minimum stem water potential (Figure 9f) and a smaller daily fluctuation of stem water potential (Figure S7f). Therefore, hydraulic capacitance plays a role in relieving xylem hydraulic stress and reducing xylem vulnerability to cavitation. During the dry-down period, larger hydraulic capacitance leads to a larger water reservoir to supply transpiration and hence requires less daily root water absorption (Q, in Figure 9g). It should be noted that when hydraulic capacitance is less than 3.0×10^{-4} m^{-1} (inset panel in Figure 9g), the plant absorbs slightly more water from soil with larger hydraulic capacitance on DOY 222. Although a larger hydraulic capacitance can supply more water, this increased water storage is smaller than the increased transpiration, and therefore more Q is needed. Stem capacitance also affects the timing of root water uptake. Larger hydraulic capacitance promotes a relatively longer period of root water uptake overnight.
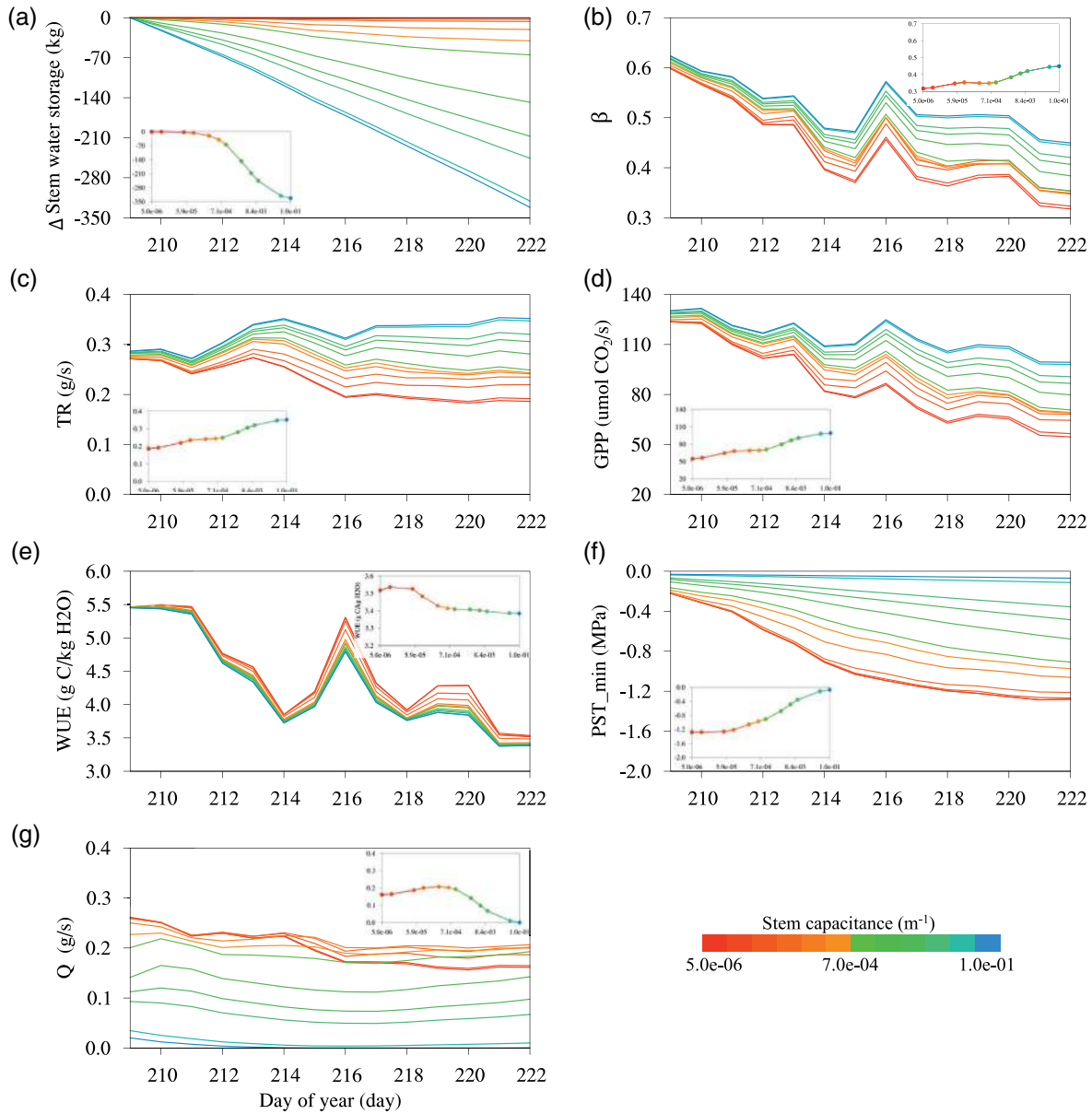
Figure 9. Daily simulations with different stem hydraulic capacitance: (a) stem water storage (values relative to the storage on DOY 209), (b) daytime plant water-stress β, (c) transpiration, (d) GPP, (e) water use efficiency (WUE), (f) minimum stem water potential (PST_min), and (g) daily total Q. The inset figures show the relationship between stem hydraulic capacitance (i.e., x axis) and the corresponding y axis value (except Figure 9g with y axis ranging from 3.2 to 3.6) on DOY 222. PHS, plant hydraulics scheme; DOY, day of year.

5. Discussion and Conclusions

In this paper, we present a PHS for use in Noah-MP. The PHS uses Darcy's law to describe the physical process of water movement from soil to root and water transportation through xylem to leaf, with explicitly representing water storage in the stem and canopy. Leaf water potential is utilized to formulate the β and hence to regulate the stomatal conductance more realistically, instead of the commonly used SHS approach, which employs soil moisture or soil water potential, as is the case in the majority of LSMs, including Noah-MP. Additional physical and measurable state variables (i.e., leaf/stem water potential and the variations of stem/canopy water storage) and flux variables (i.e., water fluxes from soil to root/stem and from stem to leaf) are represented in PHS. As such, observational constraints can be more easily incorporated in PHS than in SHSs. Many of the introduced parameters in PHS are physically measurable (e.g., $K_{s,sat}$) and could

be derived from in situ or remote-sensing measurements. The newly developed Noah-MP-PHS considers whole-plant hydraulic strategies, including hydraulic traits at leaf, stem, and root levels. Therefore, in terms of water transport and regulation, Noah-MP-PHS facilitates the transition of the soil-plant-atmosphere-continuum model from the traditional "big-leaf" concept into a "big-tree" concept.

Noah-MP-PHS improves the simulation of water and carbon in plot-level experiments, especially under dry soil conditions. The inclusion of plant hydraulics in the Noah-MP model generates a larger β (i.e., less water stress) under dry soil conditions than in three conventional SHSs, thereby enabling more realistic simulations of transpiration and GPP that closely replicate observations (Figures 2–4). Compared with the negligible diel variation of β from the default SHSs, PHS' β shows an apparent diel cycle with a maximum value at predawn and a minimum value around midday (Figure 5). Plant water stress in the default SHSs is based on soil moisture or soil water potential, which only represents the control of soil water supply and varies slowly (on the order of days and weeks). Instead, PHS utilizes leaf water potential for plant water-stress calculation, which has been shown to be a more mechanistic indicator for stomatal regulation (Manzoni, 2014; Novick et al., 2016; Sperry et al., 2017). Therefore, PHS' β responds to not only the water supply from the stem (and ultimately from soil) but also the atmospheric demand, and hence enables more realistic dynamics of water and carbon fluxes at diurnal and potentially longer timescales (Denmead & Shaw 1962; Fisher et al., 2006; Liu et al., 2020; Novick et al., 2016; Xu et al., 2016). It should be noted that the function of hydraulic redistribution was disabled in our simulations because no evidence of this phenomenon has ever been observed at UMBS (He et al., 2013). However, Noah-MP-PHS does have the ability to simulate the hydraulic redistribution process, which plays a vital role in terrestrial water and energy cycles for arid and semiarid regions (Luo et al., 2016; Ryel et al., 2002).

Noah-MP-PHS captures the asymmetrical daytime variation of GPP and transpiration under low soil moisture conditions. This is due to the asymmetrical daytime dynamics of PHS' β, with higher values in the morning than in the afternoon. PHS' β is computed based on leaf water potential, which is affected by the amount of plant water storage. Under low soil moisture conditions, compared with the afternoon, plants generally have more water storage, from the predawn recharge, in the morning (i.e., higher leaf water potential and β), and thus support higher carbon uptake. Unlike the asymmetrical variation of GPP, transpiration observations from upscaled sap flux measurements on the dry day show a nonobvious asymmetrical pattern (Figure 5). The transpiration observations are upscaled from individual tree's sap flux, which is measured at the breast height of trees. A large part of tree water storage is located between the breast height and canopy leaves where transpiration occurs. This water storage has been observed to buffer the asymmetrical transpiration variation similar to GPP under low soil water conditions, leading to a negligible asymmetrical variation of measured sap flux (Matheny et al., 2015). We adjusted the timing of upscaled sap flux (see details in section 3.1) to proxy for transpiration without changing the shape of its diel cycle, which likely cannot reflect the asymmetrical variation of actual transpiration. Future studies should consider additional improvements to proxy the sap flux as transpiration on a diel scale (e.g., using the diel pattern of GPP or flux tower evaporation measurements). The PHS simulated transpiration shows an asymmetrical diurnal variation on the dry day, which potentially captures the diurnal dynamics of actual transpiration. However, SHSs cannot capture these asymmetrical patterns of either GPP or transpiration, largely due to their negligible diel variations of β.

Noah-MP-PHS was found to successfully capture the different plant hydraulic behaviors of both red maple and red oak. Overall, simulated transpiration and stem water storage were consistent with in situ observations for these two species (Figure 6). During the dry-down period (DOY 209–222, 2014), Noah-MP-PHS successfully captured the obvious patterns of decreasing transpiration and stem water storage in red maple, and the stable transpiration and slightly reduced stem water storage in red oak (Figure 7). Additionally, the model also showed an ability to simulate the difference in Q between these two species. The red maple obtained most of its water from the second soil layer (30–60 cm), where about half of its roots exist (Figure 8). For the red oak, the majority of root water uptake came from the second soil layer (30–60 cm) during nonwater-limited conditions, transitioning to absorbing most of the water from the wetter fourth soil layer (1–10 m) as the upper three soil layers dried. These model-simulated dynamics agree well with field isotopic measurements of tree water uptake (Matheny et al., 2016). Noah-MP-PHS tree-level simulations also show the different timing of Q for these two species. Under relatively wet soil conditions, these two species

absorb most of their water during the daytime (Figure 8). As the soil dries, they start taking up more water at nighttime, which accounts for up to 50% of the total daily water uptake.

The divergent hydraulic strategies of these two species are well characterized by the trait-based parameters in PHS at the leaf (e.g., TLP), stem (e.g., saturated hydraulic conductivity), and root (e.g., RAI and rooting depth) levels. For example, the calibrated parameters of $K_{s,sat}$ and P_{50} for red maple and red oak, are comparable to the observational results of Maherali et al. (2006), reflecting their different xylem architecture. Red maple has shallow roots and our study site's well-drained soil regularly limits surface soil water resources, causing it to readily experience water stress. However, red maple is strongly isohydric, with tight stomatal regulation, and maintains a relatively stable and high leaf water potential and, hence, conservatively controls transpiration (Figure 7). Red oak is more anisohydric, characterized by its higher stomatal conductance during drought, and commonly tolerates more negative leaf water potential. This behavior of red oak is buffered by both its deep rooting depth and highly conductive xylem architecture (Matheny et al., 2016). PHS is unable to capture well the gradual recharge of stem water during the rewetting period of red maple (Figure 6). The hysteretic phenomenon occurs in the relationships between xylem water potential and conductivity during the refilling process if refilling does not, or is slow to, occur (Hacke et al., 2003; Sperry et al., 2003). In addition, the observed stem water storage shows more variability than the simulations on some nondry days. Therefore, advancement of the PHS framework should further include the mechanism to reproduce the time lag associated with vessel refilling (Mrad et al., 2018). It should be noted that the hormone abscisic acid (ABA) also contributes to regulating the stomatal aperture (Fatichi et al., 2016; Tuzet et al., 2003). Even though our PHS is capable of simulating the opposing hydraulic strategies without explicitly invoking ABA, this hormonal control could be crucial for some species and is another direction for further PHS model development (Deans et al., 2017).

These three experiments (i.e., one plot-level and two tree-level) could also provide insights for parameters upscaling from tree-level to plot-scale. The plot-level experiment represents a comprehensive hydraulic strategy characterized by all tree species at the UMBS, including aspen, birch, maple, pine, and beech (Matheny et al., 2014). Two tree-level experiments roughly express opposite hydraulic strategies ("risk-averse" versus "risk-prone") among all species at this site. Therefore, some plot-level experiment parameters are roughly intermediate to these maple and oak experiments, such as TLP and C_{stem}. It should be noted that the parameters of the plot-level experiment are closer to those of the maple experiment because observed behaviors of aspen and birch in the site are more similar to those of maple than oak. Furthermore, we could obtain the traits of plot or ecosystem levels by upscaling from species measurements. Taking UMBS as an example, we can first measure the hydraulic traits for the dominant tree species. Then, we can scale up these traits from species to plot levels by weighting species' properties, including their relative abundance, LAI and SAI (Matheny et al., 2017). Using a similar approach, Li et al. (2017) upscaled the isohydry/anisohydry from species level to grid-scale using in situ species estimates and plant species–occurrence information.

It is valuable to represent plant storage, or hydraulic capacitance, in plant hydraulics-enabled models. The representation of plant water storage affects the simulation of asymmetric diurnal variations of carbon and water fluxes. Furthermore, sensitivity experiments with plant hydraulic capacitance reveal its vital role in regulating water and carbon fluxes and WUE. Stem capacitance also helps relieve xylem hydraulic stress and reduce xylem vulnerability to cavitation during dry soil conditions (Maherali et al., 2004, 2006; Meinzer, 2003; Tyree et al., 1989). Furthermore, plant water storage enables the simulation of nocturnal plant water recharge. Nocturnal water recharge has ecophysiological significance to plants, including relieving xylem hydraulic stress and delivering nutrients (Daley & Phillips 2006; Fang et al., 2018; McDonald et al., 2002; Scholz et al., 2007; Snyder et al., 2003). Our tree-level simulations show that the nighttime recharge of red maple and red oak accounts for nearly 50% of the daily total soil-to-root water flux (Figure 8). This ratio is consistent with previous studies in which nighttime water recharge accounts for approximately 10–50% of the total daily transpiration (Carrasco et al., 2014; Scholz et al., 2008; Wang et al., 2012; Yi et al., 2017; Zhao et al., 2017). The sensitivity experiments also show that a larger stem hydraulic capacitance promotes a longer period for root water uptake at night to supply transpiration in the following daytime.

With the implemented plant hydraulics model in LSMs, the ultimate goal is for use within ESMs or numerical weather prediction (NWP) models to produce simulations at large spatial scales. One of the central challenges is how to properly represent the diversity of plant hydraulic strategies on large spatial scales. LSMs

commonly group plant species into broad categories, i.e., plant functional types (PFTs), by the phenological, environmental, and leaf morphological traits, etc. (Bonan et al., 2002; Running et al., 1994). The PFT framework has offered a simple way to deal with plant diversity (albeit with limited plant traits considered) and allowed ESMs and NWP models to efficiently simulate vegetation-climate and vegetation-weather interactions on large spatial scales (Pappas et al., 2016; Scheiter et al., 2013). However, the current PFT framework does not explicitly incorporate the whole-plant hydraulic strategy, nor does it consider plant hydraulic traits at the root, stem and leaf levels (Matheny et al., 2017). There are commonly three approaches to facilitate the incorporation of plant hydraulics into large-scale models. The first approach is to represent plant hydraulic strategies under the existing PFTs. For example, Kennedy (2020) presented a set of plant hydraulic parameters for each PFT in CLM5 to conduct global simulations. However, studies have shown that there is large divergence of plant traits within a given PFT (Konings et al., 2017; Wright et al., 2005). Alternatively, the second approach is to define new categories with similar plant hydraulic strategies either alongside or within the current PFTs. Xu et al. (2016) defined four new PFTs with discrete hydraulic traits to better reproduce vegetation dynamics in seasonally dry tropical forests. Mitchell et al. (2008) defined the "hydraulic functional types" (HFTs) to group species with different water use strategies using multiple-trait associations between 16 traits relating to water transport, WUE, and response to water deficit. The first and second approaches remain within, or are an expansion of, current PFT frameworks, and inevitably suffer similar underlying problems, including finite categories, coarse resolution, over-aggregation, and fixed plant attributes (Matheny et al., 2017; Pappas et al., 2016; Van Bodegom et al., 2012). Such disadvantages have been shown to lead to errors in water and carbon simulations and do not flexibly consider vegetation adaptation to the environment (Matthes et al., 2016; Poulter et al., 2011; Scheiter et al., 2013). Moving beyond the PFT paradigm, the third promising solution is a fully trait-based approach. Instead of classifying plants into limited categories, the calculations (e.g., water and carbon fluxes) in trait-based models are directly based on functional traits grounded by observable plant traits (Laughlin & Laughlin, 2013; Van Bodegom et al., 2014; Yang et al., 2015). These functional traits are allowed to vary in response to environmental drivers (e.g., water availability and nutrient availability) and habitat filtering/adaptation processes through the incorporation of mechanistic plant functional submodels (Van Bodegom et al., 2014; Verheijen et al., 2013). The trait-based approach is becoming a necessity for constructing the next generation of dynamic global vegetation models and has shown promising improvements in model simulations (Scheiter et al., 2013; Van Bodegom et al., 2014; Verheijen et al., 2013). Together with the emergence of multisource observations, including in situ (e.g., the TRY database, Kattge et al., 2011) and remote-sensing (e.g., airborne LiDAR-derived forest structure and functional traits, Asner et al., 2017; Fischer et al., 2019 and vegetation optical depth, Konings et al., 2019) data, as well as new technologies like machine learning (e.g., Moreno-Martínez et al., 2018; Pan et al., 2019; Verrelst et al., 2012), the trait-based approach provides a promising future for the representation of plant hydraulic and other functional traits in models with large spatial scale. In our tree-level experiments, we calibrated two sets of PHS related parameters and hence defined two types of HFT for red maple and red oak, following the second approach outlined above. This strategy allowed us to represent the distinct plant hydraulic strategies within the existing model framework.

Overall, compared to the default Noah-MP, simulations using the newly developed Noah-MP-PHS show better agreement with observations at both the plot- and tree-level. Through this new representation of plant hydraulic strategies, Noah-MP-PHS provides the capability to better understand the role of vegetation in the water and carbon cycles, energy budgets, land–atmosphere interaction, and climate feedbacks, especially under climate change conditions characterized by increased drought frequency.

Appendix A: Overview of Plant Hydraulics Model

Here, we briefly introduce the commonly used models for plant hydraulics processes (Table A1). There are three broad categories of plant hydraulics modeling strategies (McDowell et al., 2019; Mencuccini et al., 2019):

(1) PPMs treat the water movement within vascular conduits as laminar flow through pipes (Lehnebach et al., 2018; Shinozaki et al., 1964a, 1964b; McCulloh et al., 2003). These idealized vertical, parallel pipes can be either connected or disconnected from adjacent pipes depending on model assumptions. The flow through each pipe is commonly simulated by the Hagen–Poiseuille law (Mrad et al., 2018; Roderick &

Berry, 2001). Some of these models (e.g., the WBE model, Savage et al., 2008; West et al., 1999) use additional allometric scaling laws to describe vascular architecture, such as conduit taper, and further consider hydraulic trade-offs (e.g., the Botanical Network Model, Savage et al., 2010). The network model proposed by Mrad et al. (2018) based on xylem anatomy simulates lateral embolism spread, providing another solution to further explore xylem tissue hydraulic behavior and vulnerability to cavitation.

(2) EAMs conceptualize water flow through plants as being analogous to the current through an electric circuit with series of resistance and/or capacitance (Sperry et al., 1998). An EAM is based on an ordinary differential equation and has high-computational efficiency. EAMs have two subcategories: resistor model (RMs) and resistance–capacitance models (RCMs). An RM regards plant hydraulics as a resistor (or a series of resistors) to transport water flow. Sellers et al. (1986) proposed an RM in the SiB model, which included two resistors: averaged plant vascular resistance and soil–root resistance. Other examples include the plant hydraulics schemes developed by Sperry et al. (1998), the SOX scheme developed by Eller et al. (2018), and the PHS scheme in CLM5 (Kennedy et al., 2019). Besides the resistor, RCMs also consider plant water storage or capacitance, e.g., the schemes developed by Sperry et al. (1998), Steppe et al. (2006), Gentine et al. (2016), and Xu et al. (2016). The hydraulic capacitance, especially for large trees, has been demonstrated by field observation to play a critical role in regulating transpiration at both short-term and long-term scales (Matheny et al., 2015; Yan et al., 2020).

(3) PMMs assume that water movement through interconnected tracheids or the xylem resembles porous media flow (Bohrer et al., 2005; Chuang et al., 2006). A PMM typically uses the Richards equation for non-saturated porous media flow, which combines the continuity equation with Darcy's law, leading to a nonlinear partial differential equation. Therefore, these models can describe in detail the spatiotemporal dynamics of a tree's hydraulic system, but at the cost of substantial computational and parametric demands. The architecture of PMMs ranges from single beam (stem only) models (Chuang et al., 2006; Mirfenderesgi et al., 2016, 2019; Yan et al., 2020), to the FETCH model with a three-dimensional stem and branch structure (Bohrer et al., 2005), to the Xylem Water Flow (XWF) model including root, stem, and branches (Bittner et al., 2012; Janott et al., 2011).

Compared with PPMs and PMMs, EAMs require relatively few parameters and low computational demand. Therefore, they are highly suitable for use within LSMs or ESMs on a large spatial scale. In particular, RCMs consider the whole-plant hydraulic strategy as well as plant water storage, which is promising for use in LSMs.

Table A1
Commonly Used Plant Hydraulics Models and Their Key Features

	Plant hydraulics model type			
		Electric analogy model		
	Pipe model	Resistor model	Resistor–capacitance model	Porous media model
Vascular architecture assumption	Series of pipes	Electric circuit with resistance	Electric circuit with resistance and capacitance	Continuous porous media
Storage inclusion	Yes/No	No	Yes	Yes
Governing law or equation	Hagen–Poiseuille law, allometric scaling laws	Darcy's law		Richards equation
Typical model scale	Tissue level, tree level, ecosystem level	Tree level, cohort level, stand level, ecosystem level		
Computational demand	Moderate to high	Low to moderate		High
Example of evaluation data	Tree-level measurements	Sap flux, flux tower data, ecosystem-scale data		Sap flux

Table A1
Continued

	Plant hydraulics model type			
	Pipe model	Electric analogy model		Porous media model
		Resistor model	Resistor–capacitance model	
Examples	1. Pipe Model (Shinozaki et al., 1964a & b)	1. SiB (Sellers et al., 1986)	1. SPA (Williams et al., 1996)	1. PM (Chuang et al., 2006)
	2. WBE (West et al., 1999)	2. SPA (Sperry et al., 1998)	2. Dynamic Flow and Storage Model (Steppe et al., 2006)	2. FETCH (Bohrer et al., 2005)
	3. Stem Hydraulic Model (Roderick and Berry, 2001)	3. TREES (Mackay et al., 2011)	3. VIC+ (Luo et al., 2013)	3. TFS v.1-Hydro (Christoffersen et al., 2016)
	4. Botanical Network Model (Savage et al., 2010)	4. SOX (Eller et al., 2018)	4. ED2-Hydro (Xu et al., 2016)	4. XWF (Janott et al., 2011)
	5. Network Model (Mrad et al., 2018)	5. PHS in CLM5 (Kennedy et al., 2019)	5. RCL Model (Zhuang et al., 2014)	
	6. Pipe Model in HOTTER (Trugman et al., 2019b)			

Data Availability Statement

The meteorological forcing, GPP, and soil moisture observations at UMBS are available from the Ameriflux database (site-ID: US-UMB): https://ameriflux.lbl.gov/sites/siteinfo/US-UMB. The soil texture and root vertical distribution are available from He et al. (2013). The upscaled plot-level sap flux is available through Matheny et al. (2014b). The tree-level sap flux, stem water storage, leaf water potential, and other tree measurements (i.e., canopy height, sapwood area) are available through Matheny et al. (2016).

References

Allen, C. D., Macalady, A. K., Chenchouni, H., Bachelet, D., McDowell, N., Vennetier, M., et al. (2010). A global overview of drought and heat-induced tree mortality reveals emerging climate change risks for forests. *Forest Ecology and Management*, *259*(4), 660–684. http://doi.org/10.1016/j.foreco.2009.09.001

Allen, M. F. (2009). Water relations in the mycorrhizosphere. In U. Lüttge, W. Beyschlag, B. Büdel, & D. Francis (Eds.), *Progress in Botany* (Vol. 70, pp. 257–276). Berlin: Springer.

Anderegg, W. R. L., Berry, J. A., Smith, D. D., Sperry, J. S., Anderegg, L. D. L., & Field, C. B. (2012). The roles of hydraulic and carbon stress in a widespread climate-induced forest die-off. *Proceedings of the National Academy of Sciences of the United States of America*, *109*(1), 233–237. http://doi.org/10.1073/pnas.1107891109

Anderegg, W. R. L., Konings, A. G., Trugman, A. T., Kailiang, Y., Bowling, D. R., Gabbitas, R., et al. (2018). Hydraulic diversity of forests regulates ecosystem resilience during drought. *Nature*, *561*, 538–541. http://doi.org/10.1038/s41586-018-0539-7

Anderegg, W. R. L., & Venturas, M. D. (2020). Plant hydraulics play a critical role in Earth system fluxes. *New Phytologist*, *226*(6), 1535–1538. https://doi.org/10.1111/nph.16548

Asner, G. P., Martin, R. E., Knapp, D. E., Tupayachi, R., Anderson, C. B., Sinca, F., et al. (2017). Airborne laser-guided imaging spectroscopy to map forest trait diversity and guide conservation. *Science*, *355*(6323), 385–389. https://doi.org/10.1126/science.aaj1987

Ball, J. T., Woodrow, I. E., & Berry, J. A. (1987). A model predicting stomatal conductance and its contribution to the control of photosynthesis under different environmental conditions. In *Progress in photosynthesis research* (pp. 221–224). Dordrecht: Springer. https://doi.org/10.1007/978-94-017-0519-6_48

Bittner, S., Janott, M., Ritter, D., Köcher, P., Beese, F., & Priesack, E. (2012). Functional-structural water flow model reveals differences between diffuse-and ring-porous tree species. *Agricultural and Forest Meteorology*, *158*, 80–89. https://doi.org/10.1016/j.agrformet.2012.02.005

Blackman, C. J. (2018). Leaf turgor loss as a predictor of plant drought response strategies. *Tree Physiology*, *38*(5), 655–657. https://doi.org/10.1093/treephys/tpy047

Bohrer, G., Mourad, H., Laursen, T. A., Drewry, D., Avissar, R., Poggi, D., et al. (2005). Finite element tree crown hydrodynamics model (FETCH) using porous media flow within branching elements: A new representation of tree hydrodynamics. *Water Resources Research*, *41*, W11404. https://doi.org/10.1029/2005WR004181

Bonan, G. B. (2008). Forests and climate change: Forcings, feedbacks, and the climate benefits of forests. *Science*, *320*(5882), 1444–1449. http://doi.org/10.1126/science.1155121

Bonan, G. B., & Doney, S. C. (2018). Climate, ecosystems, and planetary futures: The challenge to predict life in Earth system models. *Science*, *359*(6375), eaam8328. https://doi.org/10.1126/science.aam8328

Bonan, G. B., Levis, S., Kergoat, L., & Oleson, K. W. (2002). Landscapes as patches of plant functional types: An integrating concept for climate and ecosystem models. *Global Biogeochemical Cycles*, *16*(2), 1021. https://doi.org/10.1029/2000GB001360

Bréda, N., Granier, A., Barataud, F., & Moyne, C. (1995). Soil water dynamics in an oak stand. *Plant Soil*, *172*, 17–27. https://doi.org/10.1007/BF00020856

Buckley, T. N. (2005). The control of stomata by water balance. *New Phytologist*, *168*(2), 275–292. http://doi.org/10.1111/j.1469-8137.2005.01543.x

Cai, X., Yang, Z.-L., David, C. H., Niu, G. Y., & Rodell, M. (2014). Hydrological evaluation of the Noah-MP land surface model for the Mississippi River Basin. *Journal of Geophysical Research: Atmospheres*, *119*, 23–38. https://doi.org/10.1002/2013JD020792

Cai, X., Yang, Z.-L., Fisher, J. B., Zhang, X., Barlage, M., & Chen, F. (2016). Integration of nitrogen dynamics into the Noah-MP land surface model v1. 1 for climate and environmental predictions. *Geoscientific Model Development*, *9*(1), 1–15. https://doi.org/10.5194/gmd-9-1-2016

Calvet, J. C., Noilhan, J., Roujean, J. L., Bessemoulin, P., Cabelguenne, M., Olioso, A., et al. (1998). An interactive vegetation SVAT model tested against data from six contrasting sites. *Agricultural and Forest Meteorology*, *92*(2), 73–95. https://doi.org/10.1016/S0168-1923(98)00091-4

Canadell, J., Jackson, R. B., Ehleringer, J. B., Mooney, H. A., Sala, O. E., & Schulze, E. D. (1996). Maximum rooting depth of vegetation types at the global scale. *Oecologia*, *108*(4), 583–595. https://doi.org/10.1007/BF00329030

CanadellJ. G., PatakiD. E., & Pitelka, L. F. (Eds.) (2007). *Terrestrial ecosystems in a changing world*. Berlin, Germany: Springer Science & Business Media.

Carrasco, L. O., Bucci, S. J., Francescantonio, D. D., Lezcano, O. A., Campanello, P. I., Scholz, F. G., et al. (2014). Water storage dynamics in the main stem of subtropical tree species differing in wood density, growth rate and life history traits. *Tree Physiology*, *35*, 354–365. http://doi.org/10.1093/treephys/tpu087

Chen, F., & Dudhia, J. (2001). Coupling an advanced land surface-hydrology model with the Penn State-NCAR MM5 modeling system. Part I: Model implementation and sensitivity. *Monthly Weather Review*, *129*(4), 569–585. https://doi.org/10.1175/1520-0493(2001)129<0569:CAALSH>2.0.CO;2

Choat, B., Jansen, S., Brodribb, T. J., Cochard, H., Delzon, S., Bhaskar, R., et al. (2012). Global convergence in the vulnerability of forests to drought. *Nature*, *491*, 752–756. http://doi.org/10.1038/nature11688

Christoffersen, B. O., Gloor, M., Fauset, S., Fyllas, N. M., Galbraith, D. R., Baker, T. R., et al. (2016). Linking hydraulic traits to tropical forest function in a size-structured and trait-driven model (TFS v. 1-Hydro). *Geoscientific Model Development*, *9*, 4227–4255. http://doi.org/10.5194/gmd-9-4227-2016

Chuang, Y. L., Oren, R., Bertozzi, A. L., Phillips, N., & Katul, G. G. (2006). The porous media model for the hydraulic system of a conifer tree: linking sap flux data to transpiration rate. *Ecological Modelling*, *191*(3–4), 447–468. http://doi.org/10.1016/j.ecolmodel.2005.03.027

Clapp, R. B., & Hornberger, G. M. (1978). Empirical equations for some soil hydraulic properties. *Water Resources Research*, *14*(4), 601–604. https://doi.org/10.1029/WR014i004p00601

Collatz, G. J., Ball, J. T., Grivet, C., & Berry, J. A. (1991). Physiological and environmental regulation of stomatal conductance, photosynthesis and transpiration: A model that includes a laminar boundary layer. *Agricultural and Forest Meteorology*, *54*(2–4), 107–136. https://doi.org/10.1016/0168-1923(91)90002-8

Cosgrove, B., Gochis, D., Clark, E. P., Cui, Z., Dugger, A. L., Feng, X., et al. (2016). An overview of the National Weather Service National Water Model. *AGU Fall Meeting Abstracts #H42B-05*. Washington, DC: American Geophysical Union.

Dai, A. (2013). Increasing drought under global warming in observations and models. *Nature Climate Change*, *3*(1), 52–58. http://doi.org/10.1038/nclimate1633

Daley, M. J., & Phillips, N. G. (2006). Interspecific variation in nighttime transpiration and stomatal conductance in a mixed New England deciduous forest. *Tree Physiology*, *26*(4), 411–419. https://doi.org/10.1093/treephys/26.4.411

Deans, R. M., Brodribb, T. J., & McAdam, S. A. (2017). An integrated hydraulic-hormonal model of conifer stomata predicts water stress dynamics. *Plant Physiology*, *174*(2), 478–486. https://doi.org/10.1104/pp.17.00150

Denmead, O. T., & Shaw, R. H. (1962). Availability of soil water to plants as affected by soil moisture content and meteorological conditions. *Agronomy Journal*, *54*, 385–390. https://doi.org/10.2134/agronj1962.00021962005400050005x

Dirmeyer, P. A., Gao, X., Zhao, M., Guo, Z., Oki, T., & Hanasaki, N. (2006). GSWP-2: Multimodel analysis and implications for our perception of the land surface. *Bulletin of the American Meteorological Society*, *87*(10), 1381–1398. http://doi.org/10.1175/BAMS-87-10-1381

Egea, G., Verhoef, A., & Vidale, P. L. (2011). Towards an improved and more flexible representation of water stress in coupled photosynthesis–stomatal conductance models. *Agricultural and Forest Meteorology*, *151*(10), 1370–1384. http://doi.org/10.1016/j.agrformet.2011.05.019

Eller, C. B., Rowland, L., Mencuccini, M., Rosas, T., Williams, K., Harper, A., et al. (2020). Stomatal optimisation based on xylem hydraulics (SOX) improves land surface model simulation of vegetation responses to climate. *New Phytologist*, *226*, 1622–1637. https://doi.org/10.1111/nph.16419

Eller, C. B., Rowland, L., Oliveira, R. S., Bittencourt, P. R. L., Barros, F. V., da Costa, A. C. L., et al. (2018). Modelling tropical forest responses to drought and El Niño with a stomatal optimization model based on xylem hydraulics. *Philosophical Transactions of the Royal Society B: Biological Sciences*, *373*(1760), 20170315. http://doi.org/10.1098/rstb.2017.0315

Fan, Y., Miguez-Macho, G., Jobbágy, E. G., Jackson, R. B., & Otero-Casal, C. (2017). Hydrologic regulation of plant rooting depth. *Proceedings of the National Academy of Sciences of the United States of America*, *114*(40), 10572–10577. https://doi.org/10.1073/pnas.1712381114

Fang, W., Lu, N., Zhang, Y., Jiao, L., & Fu, B. (2018). Responses of nighttime sap flow to atmospheric and soil dryness and its potential roles for shrubs on the Loess Plateau of China. *Journal of Plant Ecology*, *11*(5), 717–729. https://doi.org/10.1093/jpe/rtx042

Fatichi, S., Pappas, C., & Ivanov, V. Y. (2016). Modeling plant-water interactions: An ecohydrological overview from the cell to the global scale. *Wiley Interdisciplinary Reviews: Water*, *3*(3), 327–368. https://doi.org/10.1002/wat2.1125

Fischer, F. J., Maréchaux, I., & Chave, J. (2019). Improving plant allometry by fusing forest models and remote sensing. *New Phytologist*, *223*(3), 1159–1165. https://doi.org/10.1111/nph.15810

Fisher, R. A., Williams, M., Do Vale, R. L., Da Costa, A. L., & Meir, P. (2006). Evidence from Amazonian forests is consistent with isohydric control of leaf water potential. *Plant, Cell & Environment*, *29*(2), 151–165. https://doi.org/10.1111/j.1365-3040.2005.01407.x

Fyllas, N. M., Gloor, E., Mercado, L. M., Sitch, S., Quesada, C. A., Domingues, T. F., et al. (2014). Analysing Amazonian forest productivity using a new individual and trait-based model (TFS v. 1). *Geoscientific Model Development*, *7*, 1251–1269. https://doi.org/10.5194/gmd-7-1251-2014

Gentine, P., Guérin, M., Uriarte, M., McDowell, N. G., & Pockman, W. T. (2016). An allometry-based model of the survival strategies of hydraulic failure and carbon starvation. *Ecohydrology*, *9*(3), 529–546. https://doi.org/10.1002/eco.1654

Goldstein, G., Andrade, J. L., Meinzer, F. C., Holbrook, N. M., Cavelier, J., Jackson, P., & Celis, A. (1998). Stem water storage and diurnal patterns of water use in tropical forest canopy trees. *Plant, Cell & Environment*, *21*(4), 397–406. https://doi.org/10.1046/j.1365-3040.1998.00273.x

Good, S. P., Noone, D., & Bowen, G. (2015). Hydrologic connectivity constrains partitioning of global terrestrial water fluxes. *Science*, *349*(6244), 175–177. http://doi.org/10.1126/science.aaa5931

Grant, R. F., Wall, G. W., Kimball, B. A., Frumau, K. F. A., Pinter, P. J., Hunsaker, D. J., et al. (1999). Crop water relations under different CO_2 and irrigation: Testing of ecosys with the free air CO_2 enrichment (FACE) experiment. *Agricultural and Forest Meteorology*, *95*(1), 27–51. https://doi.org/10.1016/S0168-1923(99)00017-9Refstyled

Grant, R. F., Zhang, Y., Yuan, F., Wang, S., Hanson, P. J., & Gaumont-Guay, D. (2006). Intercomparison of techniques to model water stress effects on CO2 and energy exchange in temperate and boreal deciduous forests. *Ecological Modelling*, *196*, (3-4), 289–312. https://doi.org/10.1016/j.ecolmodel.2006.02.035

Grossiord, C., Buckley, T. N., Cernusak, L. A., Novick, K. A., Poulter, B., Siegwolf, R. T. W., et al. (2020). Plant responses to rising vapor pressure deficit. *New Phytologist*, *226*(6), 1550–1566. https://doi.org/10.1111/nph.16485

Gupta, H. V., Kling, H., Yilmaz, K. K., & Martinez, G. F. (2009). Decomposition of the mean squared error and NSE performance criteria: Implications for improving hydrological modelling. *Journal of Hydrology*, *377*(1–2), 80–91. https://doi.org/10.1016/j.jhydrol.2009.08.003

Gutschick, V. P., & Simonneau, T. (2002). Modelling stomatal conductance of field-grown sunflower under varying soil water content and leaf environment: Comparison of three models of stomatal response to leaf environment and coupling with an abscisic acid-based model of stomatal response to soil drying. *Plant, Cell & Environment*, *25*(11), 1423–1434. https://doi.org/10.1046/j.1365-3040.2002.00937.x

Hacke, U. G., & Sperry, J. S. (2003). Limits to xylem refilling under negative pressure in Laurus nobilis and Acer negundo. *Plant, Cell & Environment*, *26*(2), 303–311. https://doi.org/10.1046/j.1365-3040.2003.00962.x

He, L., Ivanov, V. Y., Bohrer, G., Thomsen, J. E., Vogel, C. S., & Moghaddam, M., et al. (2013). Temporal dynamics of soil moisture in a northern temperate mixed successional forest after a prescribed intermediate disturbance. *Agricultural and Forest Meteorology*, *180*, 22–33. https://doi.org/10.1016/j.agrformet.2013.04.014

Hickler, T., Prentice, I. C., Smith, B., Sykes, M. T., & Zaehle, S. (2006). Implementing plant hydraulic architecture within the LPJ Dynamic Global Vegetation Model. *Global Ecology and Biogeography*, *15*(6), 567–577. https://doi.org/10.1111/j.1466-8238.2006.00254.x

Hochberg, U., Rockwell, F. E., Holbrook, N. M., & Cochard, H. (2018). Iso/anisohydry: A plant-environment interaction rather than a simple hydraulic trait. *Trends in Plant Science*, *23*(2), 112–120. https://doi.org/10.1016/j.tplants.2017.11.002

Huang, C. W., Domec, J. C., Ward, E. J., Duman, T., Manoli, G., Parolari, A. J., & Katul, G. G. (2017). The effect of plant water storage on water fluxes within the coupled soil-plant system. *New Phytologist*, *213*(3), 1093–1106. https://doi.org/10.1111/nph.14273

Hunt, E. R., Jr, Running, S. W., & Federer, C. A. (1991). Extrapolating plant water flow resistances and capacitances to regional scales. *Agricultural and Forest Meteorology*, *54*(2–4), 169–195. https://doi.org/10.1016/0168-1923(91)90005-B

Janott, M., Gayler, S., Gessler, A., Javaux, M., Klier, C., & Priesack, E., et al. (2011). A one-dimensional model of water flow in soil-plant systems based on plant architecture. *Plant Soil*, *341*, 233–256. https://doi.org/10.1007/s11104-010-0639-0

Jasechko, S., Sharp, Z., Gibson, J., Jean Birks, S., Yi, Y., Fawcett, P. J., et al. (2013). Terrestrial water fluxes dominated by transpiration. *Nature*, *496*, 347–350. https://doi.org/10.1038/nature11983

Kattge, J., Diaz, S., Lavorel, S., Jean Birks, S., Yi, Y., & Fawcett, P. J., et al. (2011). TRY—A global database of plant traits. *Global Change Biology*, *17*(9), 2905–2935. https://doi.org/10.1111/j.1365-2486.2011.02451.x

Katul, G., Leuning, R., & Oren, R. (2003). Relationship between plant hydraulic and biochemical properties derived from a steady-state coupled water and carbon transport model. *Plant, Cell & Environment*, *26*(3), 339–350. https://doi.org/10.1046/j.1365-3040.2003.00965.x

Kennedy, D. (2020). *Implementing plant hydraulics in an Earth System Model and the implications for the global carbon and water cycles*. (Doctoral dissertation). New York: Columbia University. https://doi.org/10.7916/d8-9cfn-nc45

Kennedy, D., Swenson, S., Oleson, K. W., Lawrence, D. M., et al. (2019). Implementing plant hydraulics in the community land model, version 5. *Journal of Advances in Modeling Earth Systems*, *11*(2), 485–513. http://doi.org/10.1029/2018MS001500

Kling, H., Fuchs, M., & Paulin, M. (2012). Runoff conditions in the upper Danube basin under an ensemble of climate change scenarios. *Journal of Hydrology*, *424–425*, 264–277. https://doi.org/10.1016/j.jhydrol.2012.01.011

Konings, A. G., & Gentine, P. (2017). Global variations in ecosystem-scale isohydricity. *Global Change Biology*, *23*(2), 891–905. https://doi.org/10.1111/gcb.13389

Konings, A. G., Rao, K., & Steele-Dunne, S. C. (2019). Macro to micro: Microwave remote sensing of plant water content for physiology and ecology. *New Phytologist*, *223*(3), 1166–1172. https://doi.org/10.1111/nph.15808

Kumar, S. V., Peters-Lidard, C. D., Tian, Y., Lawrence, D. M., Fisher, R., Carlos, A., et al. (2006). Land information system: An interoperable framework for high resolution land surface modeling. *Environmental Modelling & Software*, *21*(10), 1402–1415. http://doi.org/10.1016/j.envsoft.2005.07.004

Laughlin, D. C., & Laughlin, D. E. (2013). Advances in modeling trait-based plant community assembly. *Trends in Plant Science*, *18*(10), 584–593. https://doi.org/10.1016/j.tplants.2013.04.012

Lehnebach, R., Beyer, R., Letort, V., & Heuret, P. (2018). The pipe model theory half a century on: A review. *Annals of Botany*, *121*(5), 773–795. http://doi.org/10.1093/aob/mcx194

Lemordant, L., Gentine, P., Swann, A. S., Cook, B. I., & Scheff, J. (2018). Critical impact of vegetation physiology on the continental hydrologic cycle in response to increasing CO2. *Proceedings of the National Academy of Sciences of the United States of America*, *115*(16), 4093–4098. https://doi.org/10.1073/pnas.1720712115

Li, L., She, D., Zheng, H., Lin, P., & Yang, Z.-L. (2020). Elucidating diverse drought characteristics from two meteorological drought indices (SPI and SPEI) in China. *Journal of Hydrometeorology*, *21*(7), 1513–1530. https://doi.org/10.1175/JHM-D-19-0290.1

Li, Y., Guan, K., Gentine, P., Konings, A. G., Meinzer, F. C., Kimball, J. S., et al. (2017). Estimating global ecosystem isohydry/anisohydry using active and passive microwave satellite data. *Journal of Geophysical Research: Biogeosciences*, *122*, 3306–3321. https://doi.org/10.1002/2017JG003958

Liang, J., Yang, Z.-L., & Lin, P. (2019). Systematic hydrological evaluation of the Noah-MP land surface model over China. *Advances in Atmospheric Sciences*, *36*(11), 1171–1187. https://doi.org/10.1007/s00376-019-9016-y

Liang, J., Yang, Z.-L., Cai, X., Lin, P., Zheng, H., & Bian, Q. (2020). Modeling the impacts of nitrogen dynamics on regional terrestrial carbon and water cycles over China with Noah-MP-CN. *Advances in Atmospheric Sciences*, *37*(7), 679–695. https://doi.org/10.1007/s00376-020-9231-6

Liu, Y., Kumar, M., Katul, G. G., Feng, X., & Konings, A. G. (2020). Plant hydraulics accentuates the effect of atmospheric moisture stress on transpiration. *Nature Climate Change*, *313*, 1–5. http://doi.org/10.1038/s41558-020-0781-5

Luo, X., Chen, J. M., Liu, J., Black, T. A., Croft, H., Staebler, R., et al. (2018). Comparison of big-leaf, two-big-leaf, and two-leaf upscaling schemes for evapotranspiration estimation using coupled carbon-water modeling. *Journal of Geophysical Research: Biogeosciences*, *123*, 207–225. https://doi.org/10.1002/2017JG003978

Luo, X., Liang, X., & Lin, J. S. (2016). Plant transpiration and groundwater dynamics in water-limited climates: Impacts of hydraulic redistribution. *Water Resources Research*, *52*, 4416–4437. https://doi.org/10.1002/2015WR017316

Luo, X., Liang, X., & McCarthy, H. R. (2013). VIC+ for water-limited conditions: A study of biological and hydrological processes and their interactions in soil-plant-atmosphere continuum. *Water Resources Research*, *49*, 7711–7732. http://doi.org/10.1002/2012WR012851

Mackay, D. S., Roberts, D. E., Ewers, B. E., Sperry, J. S., McDowell, N. G., & Pockman, W. T. (2015). Interdependence of chronic hydraulic dysfunction and canopy processes can improve integrated models of tree response to drought. *Water Resources Research*, *51*, 6156–6176. https://doi.org/10.1002/2015WR017244

Maherali, H., Moura, C. F., Caldeira, M. C., Willson, C. J., & Jackson, R. B. (2006). Functional coordination between leaf gas exchange and vulnerability to xylem cavitation in temperate forest trees. *Plant, Cell & Environment*, *29*(4), 571–583. https://doi.org/10.1111/j.1365-3040.2005.01433.x

Maherali, H., Pockman, W. T., & Jackson, R. B. (2004). Adaptive variation in the vulnerability of woody plants to xylem cavitation. *Ecology*, *85*(8), 2184–2199. https://doi.org/10.1890/02-0538

Manzoni, S. (2014). Integrating plant hydraulics and gas exchange along the drought-response trait spectrum. *Tree Physiology*, *34*(10), 1031–1034. https://doi.org/10.1093/treephys/tpu088

Matheny, A. M., Bohrer, G., Stoy, P. C., Baker, I. T., Black, A. T., Desai, A. R., et al. (2014a). Characterizing the diurnal patterns of errors in the prediction of evapotranspiration by several land-surface models: An NACP analysis. *Journal of Geophysical Research: Biogeosciences*, *119*, 1458–1473. http://doi.org/10.1002/2014JG002623

Matheny, A. M., Bohrer, G., Vogel, C. S., Morin, T. H., He, L., de Moraes Frasson, R. P., et al. (2014b). Species-specific transpiration responses to intermediate disturbance in a northern hardwood forest. *Journal of Geophysical Research: Biogeosciences*, *119*, 2292–2311. http://doi.org/10.1002/2014JG002804

Matheny, A. M., Bohrer, G., Garrity, S. R., Morin, T. H., Howard, C. J., & Vogel, C. S. (2015). Observations of stem water storage in trees of opposing hydraulic strategies. *Ecosphere*, *6*(9), 1–13. http://doi.org/10.1890/ES15-00170.1

Matheny, A. M., Fiorella, R. P., Bohrer, G., Poulsen, C. J., Morin, T. H., Wunderlich, A., et al. (2016). Contrasting strategies of hydraulic control in two codominant temperate tree species. *Ecohydrology*, *10*(3), e1815. https://doi.org/10.1002/eco.1815

Matheny, A. M., Mirfenderesgi, G., & Bohrer, G. (2017). Trait-based representation of hydrological functional properties of plants in weather and ecosystem models. *Plant Diversity*, *39*(1), 1–12. http://doi.org/10.1016/j.pld.2016.10.001

Matthes, J. H., Goring, S., Williams, J. W., & Dietze, M. C. (2016). Benchmarking historical CMIP5 plant functional types across the Upper Midwest and Northeastern United States. *Journal of Geophysical Research: Biogeosciences*, *121*, 523–535. https://doi.org/10.1002/2015JG003175

McCulloh, K. A., Domec, J.-C., Johnson, D. M., Smith, D. D., & Meinzer, F. C. (2019). A dynamic yet vulnerable pipeline: Integration and coordination of hydraulic traits across whole plants. *Plant, Cell & Environment*, *42*(10), 2789–2807. http://doi.org/10.1111/pce.13607

McCulloh, K., Sperry, J., & Adler, F. (2003). Water transport in plants obeys Murray's law. *Nature*, *421*, 939–942. https://doi.org/10.1038/nature01444

McDonald, E. P., Erickson, J. E., & Kruger, E. L. (2002). Research note: Can decreased transpiration limit plant nitrogen acquisition in elevated CO2?. *Functional Plant Biology*, *29*(9), 1115–1120. https://doi.org/10.1071/FP02007

McDowell, N. G., Brodribb, T. J., & Nardini, A. (2019). Hydraulics in the 21st century. *New Phytologist*, *224*(2), 537–542. http://doi.org/10.1111/nph.16151

McDowell, N. G., Pockman, W. T., Allen, C. D., Breshears, D. D., Cobb, N., Kolb, T., et al. (2008). Mechanisms of plant survival and mortality during drought: Why do some plants survive while others succumb to drought?. *The New Phytologist*, *178*, 719–739. http://doi.org/10.1111/j.1469-8137.2008.02436.x

Meinzer, F. C., James, S. A., Goldstein, G., & Woodruff, D. (2003). Whole-tree water transport scales with sapwood capacitance in tropical forest canopy trees. *Plant, Cell & Environment*, *26*(7), 1147–1155. https://doi.org/10.1046/j.1365-3040.2003.01039.x

Mencuccini, M., Manzoni, S., & Christoffersen, B. (2019). Modelling water fluxes in plants: from tissues to biosphere. *New Phytologist*, *8*, 367. http://doi.org/10.1111/nph.15681

Mirfenderesgi, G., Bohrer, G., Matheny, A. M., Fatichi, S., de Moraes Frasson, R. P., & Schäfer, K. V. R. (2016). Tree level hydrodynamic approach for resolving aboveground water storage and stomatal conductance and modeling the effects of tree hydraulic strategy. *Journal of Geophysical Research: Biogeosciences*, *121*, 1792–1813. https://doi.org/10.1002/2016JG003467

Mirfenderesgi, G., Matheny, A. M., & Bohrer, G. (2019). Hydrodynamic trait coordination and cost-benefit trade-offs throughout the isohydric–anisohydric continuum in trees. *Ecohydrology*, *12*(1), e2041. http://doi.org/10.1002/eco.2041

Mitchell, P. J., Veneklaas, E. J., Lambers, H., & Burgess, S. S. (2008). Using multiple trait associations to define hydraulic functional types in plant communities of south-western Australia. *Oecologia*, *158*(3), 385–397. https://doi.org/10.1007/s00442-008-1152-5

Moreno-Martínez, Á., Camps-Valls, G., Kattge, J., Robinson, N., Reichstein, M., Bodegomo, P., et al. (2018). A methodology to derive global maps of leaf traits using remote sensing and climate data. *Remote Sensing of Environment*, *218*, 69–88. https://doi.org/10.1016/j.rse.2018.09.006

Mrad, A., Domec, J. C., Huang, C. W., Lens, F., & Katul, G. (2018). A network model links wood anatomy to xylem tissue hydraulic behaviour and vulnerability to cavitation. *Plant, cell & environment*, *41*(12), 2718–2730. http://doi.org/10.1111/pce.13415

Niu, G.-Y., Yang, Z.-L., Mitchell, K.-E., Chen, F., Ek, M. B., Barlage, M., et al. (2011). The community Noah land surface model with multiparameterization options (Noah-MP): 1. Model description and evaluation with local-scale measurements. *Journal of Geophysical Research: Atmospheres*, *116*, D12109. http://doi.org/10.1029/2010JD015139

Novick, K. A., Ficklin, D. L., Stoy, P. C., Williams, C. A., Bohrer, G.,Oishi, A. C., et al. (2016). The increasing importance of atmospheric demand for ecosystem water and carbon fluxes. *Nature Climate Change*, *6*(11), 1023–1027. https://doi.org/10.1038/nclimate3114

Oleson, K., Dai, Y., Bonan, G. B., Bosilovichm, M., Dickinson, M., Dirmeyer, R., et al. (2004). *Technical description of the Community Land Model (CLM) (No. NCAR/TN-461+STR)*. University Corporation for Atmospheric Research. https://doi.org/10.5065/D6N877R0

Oren, R., Sperry, J. S., Katul, G. G., Pataki, D. E., Ewers, B. E., Phillips, N., & Schäfer, K. V. R. (1999). Survey and synthesis of intra-and interspecific variation in stomatal sensitivity to vapour pressure deficit. *Plant, Cell & Environment*, *22*(12), 1515–1526. https://doi.org/10.1046/j.1365-3040.1999.00513.x

Pan, B., Hsu, K., AghaKouchak, A., & Sorooshian, S. (2019). Improving precipitation estimation using convolutional neural network. *Water Resources Research*, *55*, 2301–2321. https://doi.org/10.1029/2018WR024090

Pappas, C., Fatichi, S., & Burlando, P. (2016). Modeling terrestrial carbon and water dynamics across climatic gradients: Does plant trait diversity matter?. *New Phytologist*, *209*(1), 137–151. http://doi.org/10.1111/nph.13590

Pavlick, R., Drewry, D. T., Bohn, K., Reu, B., & Kleidon, A. (2013). The Jena Diversity-Dynamic Global Vegetation Model (JeDi-DGVM): A diverse approach to representing terrestrial biogeography and biogeochemistry based on plant functional trade-offs. *Biogeosciences*, *10*, 4137–4177. http://hdl.handle.net/11858/00-001M-0000-0013-F551-6

Pockman, W. T., & Sperry, J. S. (2000). Vulnerability to xylem cavitation and the distribution of Sonoran desert vegetation. *American Journal of Botany*, *87*, 1287–1299. http://doi.org/10.2307/2656722

Poulter, B., Ciais, P., Hodson, E., Lischke, H.,Maignan, F., Plummer, S., & Zimmermann, N. E. (2011). Plant functional type mapping for earth system models. *Geoscientific Model Development*, *4*(4), 993–1010. https://doi.org/10.5194/gmd-4-993-2011

Powell, T. L., Galbraith, D. R., Christoffersen, B. O., Harper, A., Imbuzeiro, H. M. A., Rowland, L., et al. (2013). Confronting model predictions of carbon fluxes with measurements of Amazon forests subjected to experimental drought. *New Phytologist*, *200*(2), 350–365. http://doi.org/10.1111/nph.12390

Reichstein, M., Bahn, M., Mahecha, M. D., Kattge, J., & Baldocchi, D. D. (2014). Linking plant and ecosystem functional biogeography. *Proceedings of the National Academy of Sciences of the United States of America*, *111*(38), 13697–13702. https://doi.org/10.1073/pnas.1216065111

Reid, D. E., Silins, U., Mendoza, C., & Lieffers, V. J. (2005). A unified nomenclature for quantification and description of water conducting properties of sapwood xylem based on Darcy's law. *Tree Physiology*, *25*(8), 993–1000. https://doi.org/10.1093/treephys/25.8.993

Roderick, M. L., & Berry, S. L. (2001). Linking wood density with tree growth and environment: a theoretical analysis based on the motion of water. *New Phytologist*, *149*(3), 473–485. http://doi.org/10.1046/j.1469-8137.2001.00054.x

Running, S. W., Loveland, T. R., & Pierce, L. L. (1994). A vegetation classification logic-based on remote-sensing for use in global biogeochemical models. *Ambio*, *23*(1), 77–81.

Ryel, R., Caldwell, M., Yoder, C., Or, D., & Leffler, A. (2002). Hydraulic redistribution in a stand of Artemisia tridentata: Evaluation of benefits to transpiration assessed with a simulation model. *Oecologia*, *130*(2), 173–184. https://doi.org/10.1007/s004420100794

Savage, V. M., Bentley, L. P., Enquist, B. J., Sperry, J. S., Smith, D. D., Reich, P. B., & von Allmen, E. I. (2010). Hydraulic trade-offs and space filling enable better predictions of vascular structure and function in plants. *Proceedings of the National Academy of Sciences of the United Stated of America*, *107*(52), 22722–22727. https://doi.org/10.1073/pnas.1012194108

Savage, V. M., Deeds, E. J., & Fontana, W. (2008). Sizing Up Allometric Scaling Theory. *PLOS Computational Biology*, *4*(9), e1000171. http://doi.org/10.1371/journal.pcbi.1000171

Saxton, K. E., Rawls, W., Romberger, J. S., & Papendick, R. I. (1986). Estimating generalized soil-water characteristics from texture. *Soil science society of America Journal*, *50*(4), 1031–1036. https://doi.org/10.2136/sssaj1986.03615995005000040039x

Scheiter, S., Langan, L., & Higgins, S. I. (2013). Next-generation dynamic global vegetation models: Learning from community ecology. *New Phytologist*, *198*(3), 957–969. https://doi.org/10.1111/nph.12210

Schlesinger, W. H., & Jasechko, S. (2014). Transpiration in the global water cycle. *Agricultural and Forest Meteorology*, *189–190*, 115–117. https://doi.org/10.1016/j.agrformet.2014.01.011

Scholz, F. C., Bucci, S. J., Goldstein, G., Franco, F. C., & Miralles-Wilhelm, F. (2008). Temporal dynamics of stem expansion and contraction in savanna trees: withdrawal and recharge of stored water. *Tree Physiology*, *28*(3), 469–480. https://doi.org/10.1093/treephys/28.3.469

Scholz, F. G., Bucci, S. J., Goldstein, G., Meinzer, F. C., Franco, A. C., & Miralles-Wilhelm, F. (2007). Removal of nutrient limitations by long-term fertilization decreases nocturnal water loss in savanna trees. *Tree Physiology*, *27*(4), 551–559. https://doi.org/10.1093/treephys/27.4.551

Sellers, P. J., Mintz, Y. C. S. Y., Sud, Y. E. A., & Dalcher, A. (1986). A simple biosphere model (SiB) for use within general circulation models. *Journal of the Atmospheric Sciences*, *43*(6), 505–531. https://doi.org/10.1175/1520-0469(1986)043<0505:ASBMFU>2.0.CO;2

Sellers, P. J., Randall, D. A., Collatz, G. J., Berry, J. A., Dazlich, D. A., Zhang, C., et al. (1996). A revised land surface parameterization (SiB2) for atmospheric GCMs. Part I: Model formulation. *Journal of Climate*, *9*(4), 676–705. https://doi.org/10.1175/1520-0442(1996)009%3C0676:ARLSPF%3E2.0.CO;2

Shinozaki, K., Yoda, K., Hozumi, K., & Kira, T. (1964a). A quantitative analysis of plant form-the pipe model theory: I. Basic analyses. *Japanese Journal of ecology*, *14*(3), 97–105. https://doi.org/10.18960/seitai.14.3_97

Shinozaki, K, Yoda, K, Hozumi, K, & Kira, T (1964b). A quantitative analysis of plant form–the pipe model theory. II. Further evidence of the theory and its application in forest ecology. *Japanese Journal of Ecology*, *14*, 133–139. https://doi.org/10.18960/seitai.14.4_133

Sitch, S., Friedlingstein, P., Gruber, N., Jones, S. D., Murray-Tortarolo, G., Ahlström, A., Doney, S. C., et al. (2015). Recent trends and drivers of regional sources and sinks of carbon dioxide. *Biogeosciences*, *12*(3), 653–679. http://doi.org/10.5194/bg-12-653-2015

Skamarock, W. C., Klemp, J. B., Dudhia, J., Gill, D. O., Liu, Z., Berner, J., et al. (2019). *A description of the Advanced Research WRF Model Version 4*. (No. NCAR/TN-556+STR). http://doi.org/10.5065/1dfh-6p97

Skelton, R. P., West, A. G., & Dawson, T. E. (2015). Predicting plant vulnerability to drought in biodiverse regions using functional traits. *Proceedings of the National Academy of Sciences of the United States of America*, *112*, 5744–5749. http://doi.org/10.1073/pnas.1503376112

Snyder, K. A., Richards, J. H., & Donovan, L. A. (2003). Night-time conductance in C3 and C4 species: Do plants lose water at night?. *Journal of Experimental Botany*, *54*(383), 861–865. https://doi.org/10.1093/jxb/erg082

Sperry, J. S. (2000). Hydraulic constraints on plant gas exchange. *Agricultural and Forest Meteorology*, *104*(1), 13–23. https://doi.org/10.1016/S0168-1923(00)00144-1

Sperry, J. S., Adler, F. R., Campbell, G. S., & Comstock, J. P. (1998). Limitation of plant water use by rhizosphere and xylem conductance: results from a model. *Plant, Cell & Environment*, *21*(4), 347–359. https://doi.org/10.1046/j.1365-3040.1998.00287.x

Sperry, J. S., Stiller, V., & Hacke, U. G. (2003). Xylem hydraulics and the soil–plant–atmosphere continuum. *Agronomy Journal*, *95*(6), 1362–1370. https://doi.org/10.2134/agronj2003.1362

Sperry, J. S., Venturas, M. D., Anderegg, W. R., Mencuccini, M., Scott Mackay, D., Wang, Y., & Love, D. M., (2017). Predicting stomatal responses to the environment from the optimization of photosynthetic gain and hydraulic cost. *Plant, Cell & Environment*, *40*(6), 816–830. https://doi.org/10.1111/pce.12852

Sperry, J. S., Wang, Y., Wolfe, B. T., Scott Mackay, D., Anderegg, W. R. L., McDowel, N. G., & Pockman, W. T. (2016). Pragmatic hydraulic theory predicts stomatal responses to climatic water deficits. *New Phytologist*, *212*(3), 577–589. https://doi.org/10.1111/nph.14059

Steppe, K., De Pauw, D. J., Lemeur, R., & Vanrolleghem, P. A. (2006). A mathematical model linking tree sap flow dynamics to daily stem diameter fluctuations and radial stem growth. *Tree physiology*, *26*(3), 257–273. https://doi.org/10.1093/treephys/26.3.257

Thomsen, J., Bohrer, G., Matheny, A. M., Ivanov, V. Y., He, L., Renninger, H. J., & Schäfer, K. V. Y. (2013). Contrasting hydraulic strategies during dry soil conditions in Quercus rubra and Acer rubrum in a sandy site in Michigan. *Forests*, *4*, 1106–1120. https://doi.org/10.3390/f4041106

Trugman, A. T., Anderegg, L. D., Wolfe, B. T., Wang, Y., Venturas, M., & Anderegg, W. R. L. (2019b). Climate and plant trait strategies determine tree carbon allocation to leaves and mediate future forest productivity. *Global Change Biology*, *25*(10), 3395–3405. https://doi.org/10.1111/gcb.14680

Trugman, A. T., Anderegg, L. D. L., Sperry, J. S., Wang, Y., Venturas, M., & Anderegg, W. R. L. (2019a). Leveraging plant hydraulics to yield predictive and dynamic plant leaf allocation in vegetation models with climate change. *Global Change Biology*, *25*(12), 4008–4021. http://doi.org/10.1111/gcb.14814

Trugman, A. T., Medvigy, D., Mankin, J. S., & Anderegg, W. R. L. (2018). Soil moisture stress as a major driver of carbon cycle uncertainty. *Geophysical Research Letters*, *45*, 6495–6503. https://doi.org/10.1029/2018GL078131

Tuzet, A., Perrier, A., & Leuning, R. (2003). A coupled model of stomatal conductance, photosynthesis and transpiration. *Plant, Cell & Environment*, *26*(7), 1097–1116. http://doi.org/10.1046/j.1365-3040.2003.01035.x

Tyree, M. T., & Sperry, J. S. (1989). Vulnerability of xylem to cavitation and embolism. *Annual Review of Plant Biology*, *40*(1), 19–36. https://doi.org/10.1146/annurev.pp.40.060189.000315

van Bodegom, P. M., Douma, J. C., & Verheijen, L. M. (2014). A fully traits-based approach to modeling global vegetation distribution. *Proceedings of the National Academy of Sciences*, *111*(38), 13733–13738. https://doi.org/0.1073/pnas.1304551110

Van Bodegom, P. M., Douma, J. C., Witte, J. P. M., Ordoñez, J. C., Bartholomeus, R. P., & Aerts, R. (2012). Going beyond limitations of plant functional types when predicting global ecosystem–atmosphere fluxes: Exploring the merits of traits-based approaches. *Global Ecology and Biogeography*, *21*(6), 625–636. https://doi.org/10.1111/j.1466-8238.2011.00717.x

Verheijen, L. M., Brövkin, V., Aerts, R., Bonisch, G., Cornelissen, J. H. C., Kattge, J., et al. (2013). Impacts of trait variation through observed trait-climate relationships on performance of an Earth system model: A conceptual analysis. *Biogeosciences*, *10*, 5497–5515. https://doi.org/10.5194/bg-10-5497-2013

Verhoef, A., & Egea, G. (2014). Modeling plant transpiration under limited soil water: Comparison of different plant and soil hydraulic parameterizations and preliminary implications for their use in land surface models. *Agricultural and Forest Meteorology*, *191*, 22–32. http://doi.org/10.1016/j.agrformet.2014.02.009

Verrelst, J., Muñoz, J., Alonso, L., Pablo, J., GustavoCamps-Valls, R., & Moreno, J. (2012). Machine learning regression algorithms for biophysical parameter retrieval: Opportunities for Sentinel-2 and-3. *Remote Sensing of Environment*, *118*, 127–139. https://doi.org/10.1016/j.rse.2011.11.002

Wang, H., Zhao, P., Hölscher, D., Lu, P., Cai, X. A., & Zeng, X. P. (2012). Nighttime sap flow of *Acacia mangium* and its implications for nighttime transpiration and stem water storage. *Journal of Plant Ecology*, *5*(3), 294–304. https://doi.org/10.1093/jpe/rtr025

Wang, H., Zhao, P., Wang, Q., Cai, X., Ma, L., Rao, X., & Zeng, X. (2008). Nocturnal sap flow characteristics and stem water recharge of *Acacia mangium*. *Frontiers of Forestry in China*, *3*(1), 72–78. https://doi.org/10.1007/s11461-008-0005-z

West, G. B., Brown, J. H., & Enquist, B. J. (1999). A general model for the structure and allometry of plant vascular systems. *Nature*, *400*(6745), 664–667. https://doi.org/10.1038/23251

Williams, M., Rastetter, E. B., Fernandes, D. N., Goulden, M. L., Wofsy, S. C., Shaver, G. R., et al. (1996). Modelling the soil-plant-atmosphere continuum in a Quercus–Acer stand at Harvard Forest: the regulation of stomatal conductance by light, nitrogen and soil/plant hydraulic properties. *Plant, Cell & Environment*, *19*(8), 911–927. https://doi.org/10.1111/j.1365-3040.1996.tb00456.x

Wright, I. J., Reich, P. B., Cornelissen, J. H., Falster, D. S., Garnier, E., Hikosaka, K., et al. (2005). Assessing the generality of global leaf trait relationships. *New Phytologist*, *166*(2), 485–496. https://doi.org/10.1111/j.1469-8137.2005.01349.x

Wu, G., Guan, K., Li, Y., Novick, K. A., Feng, X., McDowell, N. G.,Konings, A. G., et al. (2020). *Interannual variability of ecosystem iso/anisohydry is regulated by environmental dryness*. New Phytologist, *229*(5), 2562–2575. https://doi.org/10.1111/nph.17040

Wullschleger, S. D., Epstein, H. E., Box, E. O., Euskirchen, E. S., Goswami, S., Iversen, C. M., et al. (2014). Plant functional types in Earth system models: past experiences and future directions for application of dynamic vegetation models in high-latitude ecosystems. *Annals of Botany*, *114*(1), 1–16. https://doi.org/10.1093/aob/mcu077

Xia, Y., Mitchell, K., Ek, M., Sheffield, J., Cosgrove, B., Wood, E., et al. (2012). Continental-scale water and energy flux analysis and validation for the North American Land Data Assimilation System project phase 2 (NLDAS-2): 1. Intercomparison and application of model products. *Journal of Geophysical Research: Atmospheres*, *117*, D03109. https://doi.org/10.1029/2011JD016048

Xu, X., Medvigy, D., Powers, J. S., Becknell, J. M., & Guan, K. (2016). Diversity in plant hydraulic traits explains seasonal and inter-annual variations of vegetation dynamics in seasonally dry tropical forests. *New Phytologist*, *212*(1), 80–95. https://doi.org/10.1111/nph.14009

Xue, Y., Sellers, P. J., Kinter, J. L., & Shukla, J. (1991). A simplified biosphere model for global climate studies. *Journal of Climate*, *4*(3), 345–364. https://doi.org/10.1175/1520-0442(1991)004<0345:ASBMFG>2.0.CO;2

Yan, B., Mao, J., Dickinson, R. E., Thornton, P. E., Shi, X., Ricciuto, D. M., et al. (2020). Modelling tree stem-water dynamics over an Amazonian rainforest. *Ecohydrology*, *13*(1), e2180. https://doi.org/10.1002/eco.2180

Yang, Y., Zhu, Q., Peng, C., Wang, H., & Chen, H. (2015). From plant functional types to plant functional traits: A new paradigm in modelling global vegetation dynamics. *Progress in Physical Geography*, *39*(4), 514–535. https://doi.org/10.1177/0309133315582018

Yang, Z.-L., & Dickinson, R. E. (1996). Description of the biosphere-atmosphere transfer scheme (BATS) for the soil moisture workshop and evaluation of its performance. *Global and Planetary Change*, *13*(1–4), 117–134. https://doi.org/10.1016/0921-8181(95)00041-0

Yang, Z.-L., Niu, G.-Y., Mitchell, K. E., Chen, F, Ek, M. B., Barlage, M., et al. (2011). The community Noah land surface model with multiparameterization options (Noah-MP): 2. Evaluation over global river basins. *Journal of Geophysical Research: Atmospheres*, *116*, D12110. http://doi.org/10.1029/2010JD015140

Yi, K., Dragoni, D., Phillips, R. P., Roman, D. T., & Novick, K. A. (2017). Dynamics of stem water uptake among isohydric and anisohydric species experiencing a severe drought. *Tree Physiology*, *37*(10), 1379–1392. http://doi.org/10.1093/treephys/tpw126

Yuan, H., Dai, Y., Xiao, Z., Ji, D., & Shangguan, W. (2011). Reprocessing the MODIS Leaf Area Index products for land surface and climate modelling. *Remote Sensing of Environment*, *115*(5), 1171–1187. https://doi.org/10.1016/j.rse.2011.01.001

Zhao, X., Zhao, P., Zhang, Z., et al. (2017). Culm age and rhizome affects night-time water recharge in the bamboo Phyllostachys pubescens. *Frontiers in plant science*, *8*, 1928. https://doi.org/10.3389/fpls.2017.01928

Zhu, S. D., Chen, Y. J., & Cao, K. F. (2018). Leaf turgor loss point is correlated with drought tolerance and leaf carbon economics traits. *Tree Physiology*, *38*(5), 658–663. https://doi.org/10.1093/treephys/tpy013

Zhuang, J., Yu, G. R., & Nakayama, K. (2014). A series RCL circuit theory for analyzing non-steady-state water uptake of maize plants. *Scientific reports*, *4*(1), 482. https://doi.org/10.1038/srep06720

Zheng, H., Yang, Z.-L., Lin, P., Wei, J., Wu, W.-Y., Li, L., et al. (2019). On the sensitivity of the precipitation partitioning into evapotranspiration and runoff in land surface parameterizations. *Water Resources Research*, *55*, 95–111. https://doi.org/10.1029/2017WR022236

Zheng, H., Yang, Z.-L., Lin, P., Wu, W. Y., Li, L., Xu, L., et al. (2020). Falsification-oriented signature-based evaluation for guiding the development of land surface models and the enhancement of observations. *Journal of Advances in Modeling Earth Systems*, *2*, e2020M-S002132 https://doi.org/10.1029/2020MS002132